

NRL Report 7385

Preliminary Investigation
of Thomson Scatter Radar as an Aid
to High-Frequency Direction Finding

J.M. Goodman, E.L. Gott, K.W. Morin
M.W. Lehman and E. Piernik

Radar Geophysics Branch
Radar Division

June 6, 1972

Approved for public release; distribution
unlimited

DOCUMENT CONTROL DATA - R & D₁

(Security classification of title, body of abstract and indexing annotation must be entered when the overall report is classified)

1. ORIGINATING ACTIVITY (Corporate author)		2a. REPORT SECURITY CLASSIFICATION	
Naval Research Laboratory Washington, D.C. 20390		Unclassified	
		2b. GROUP	
3. REPORT TITLE			
PRELIMINARY INVESTIGATION OF THOMSON SCATTER RADAR AS AN AID TO HIGH-FREQUENCY DIRECTION FINDING			
4. DESCRIPTIVE NOTES (Type of report and inclusive dates)			
A final report on one phase of the problem			
5. AUTHOR(S) (First name, middle initial, last name)			
John M. Goodman, Edgar L. Gott, Kenneth W. Morin, Melvin W. Lehman, and Edward Piernik			
6. REPORT DATE		7a. TOTAL NO. OF PAGES	7b. NO. OF REFS
June 6, 1972		56	19
8a. CONTRACT OR GRANT NO.		9a. ORIGINATOR'S REPORT NUMBER(S)	
NRL Problem R07-28		NRL Report 7385	
b. PROJECT NO.			
RR 008-01-41-5557		9b. OTHER REPORT NO(S) (Any other numbers that may be assigned this report)	
c.			
d.			
10. DISTRIBUTION STATEMENT			
Approved for public release; distribution unlimited.			
11. SUPPLEMENTARY NOTES		12. SPONSORING MILITARY ACTIVITY	
		Department of the Navy Office of Naval Research Arlington, Virginia 22217	
13. ABSTRACT			
<p>During 1970-71, a set of experiments was carried out to determine the usefulness of Thomson scatter as an aid to direction finding. Twenty one experiments were conducted, and approximately 102 hours of radar operation were involved. Although the radar elevation angles employed were quite small (between 10 and 20 degrees), useful Faraday-rotation data were obtained, and skeleton electron-density profiles were constructed. A refined method for deducing the electron density and the ratio T_e/T_i is outlined in this report.</p> <p>It is shown that Thomson scatter can detect traveling ionospheric disturbances over a highly oblique radar ray trajectory. The format chosen to display the disturbances is a plot of Faraday rotation isopleths which exhibit height fluctuations as a function of time. Near the peak of the F layer the isopleths are obscured by Faraday dispersion; nevertheless it is possible to obtain some information by monitoring fluctuations in the position of the $F2$ maximum. From a consideration of the theory of neutral gravity waves, it is possible to relate F-layer height fluctuations to electron-density gradients in the horizontal plane. The knowledge of such gradients may be used to predict bearing-angle fluctuations induced by traveling ionospheric disturbances.</p>			

DD FORM 1 NOV 65 1473 (PAGE 1)

S/N 0101-807-6801

53

Security Classification

14. KEY WORDS	LINK A		LINK B		LINK C	
	ROLE	WT	ROLE	WT	ROLE	WT
Thomson scatter Faraday rotation Traveling ionospheric disturbances Internal gravity waves Electron density fluctuations Direction finding						

CONTENTS

Abstract	ii
Problem Status	ii
Authorization	ii
INTRODUCTION	1
SIMPLIFIED THEORY AND MEASUREMENT TECHNIQUE	3
FARADAY DISPERSION	5
INITIAL BACKSCATTER PROFILES	6
SEARCH FOR TRAVELING IONOSPHERIC DISTURBANCES	10
Skeleton Electron-Density Profiles	10
Faraday-Rotation Isopleths	11
DISCUSSION OF THE THEORY OF LAYER HEIGHT FLUCTUATIONS	23
COMPARISON OF OBSERVED BEARING-ANGLE FLUCTUATIONS AND THOSE PREDICTED USING THOMSON SCATTER	28
Measurements	29
Transformation of Wave Parameters into Predicted Bearing Angle	42
Concluding Remarks	47
SUMMARY	49
REFERENCES	50

ABSTRACT

During 1970-71, a set of experiments was carried out to determine the usefulness of Thomson scatter as an aid to direction finding. Twenty one experiments were conducted, and approximately 102 hours of radar operation were involved. Although the radar elevation angles employed were quite small (between 10 and 20 degrees), useful Faraday-rotation data were obtained, and skeleton electron-density profiles were constructed. A refined method for deducing the electron density and the ratio T_e/T_i is outlined in this report.

It is shown that Thomson scatter can detect traveling ionospheric disturbances over a highly oblique radar ray trajectory. The format chosen to display the disturbances is a plot of Faraday rotation isopleths which exhibit height fluctuations as a function of time. Near the peak of the F layer the isopleths are obscured by Faraday dispersion; nevertheless it is possible to obtain some information by monitoring fluctuations in the position of the $F2$ maximum. From a consideration of the theory of neutral gravity waves, it is possible to relate F -layer height fluctuations to electron-density gradients in the horizontal plane. The knowledge of such gradients may be used to predict bearing-angle fluctuations induced by traveling ionospheric disturbances.

PROBLEM STATUS

A final report on one phase of the NRL Problem.

AUTHORIZATION

NRL Problem R07-28*
Project RR 008-01-41-5557

Manuscript submitted January 5, 1972.

*All of the experimental effort and the majority of the data analysis which was carried out and discussed in this report was conducted under NRL Problem R06-25. Recent analysis and the cost of preparing the report has been borne by NRL Problem R07-28.

PRELIMINARY INVESTIGATION OF THOMSON SCATTER RADAR AS AN AID TO HIGH-FREQUENCY DIRECTION FINDING

INTRODUCTION

It is well established that electron-density profiles of the ionosphere may be obtained through use of powerful radar systems (1), and extensive experimental effort has been devoted to this effort for almost a decade. The technique generally requires a radar system with a substantial power-aperture product, and the Randle Cliff Radar (RCR) located at the Chesapeake Bay Division (CBD) of the Naval Research Laboratory ($38^{\circ} 39' 37''$ N, $76^{\circ} 32' 9.4''$ W) satisfies this requirement. The RCR is nominally* a 5-MW-peak radar and uses the 150-ft-diameter dish antenna shown in Fig. 1. The pertinent RCR system parameters are given in Table 1. The potential of the RCR for performing useful Thomson scatter measurements has been discussed in an earlier NRL report (2) and will not be pursued here. However, one of the main points made in that report was the following: Useful measurements at Randle Cliff could indeed be made at 138.6 MHz, especially when employing the Faraday-rotation phenomenon. In fact, the RCR operating frequency is approximately optimum for conducting Thomson scatter studies using Faraday rotation at middle latitudes (3-4). Recently, NRL efforts in deducing *F*-region profiles at Randle Cliff have been reported (5-8), but due to a troublesome clutter environment at CBD, the resultant profiles do not extend significantly below 200 km.

Table 1. Naval Research Laboratory
Randle Cliff Radar (RCR) characteristics

Latitude	$38^{\circ} 39' 37.1''$ N
Longitude	$76^{\circ} 32' 9.4''$ W
Magnetic latitude	$\sim 50^{\circ}$
Frequency	138.6 MHz
Antenna	150 ft dia. dish (~ 46 m)
System noise temperature	1590° K
Beamwidth	3.6°
Antenna gain	34.6 dB
Receiver bandwidth	23 kHz
Peak power	~ 5 MW
Average power	~ 50 kW (duty cycle: 1 per cent max.)
Pulse width	5-1000 μ s (variable)

*During the course of these experiments the actual transmitter power was reduced from the rated value, due to a slowly deteriorating final-amplifier tube. The measured peak power dropped from 3.5 to 1.0 MW between the early part of 1970 and the summer of 1971.

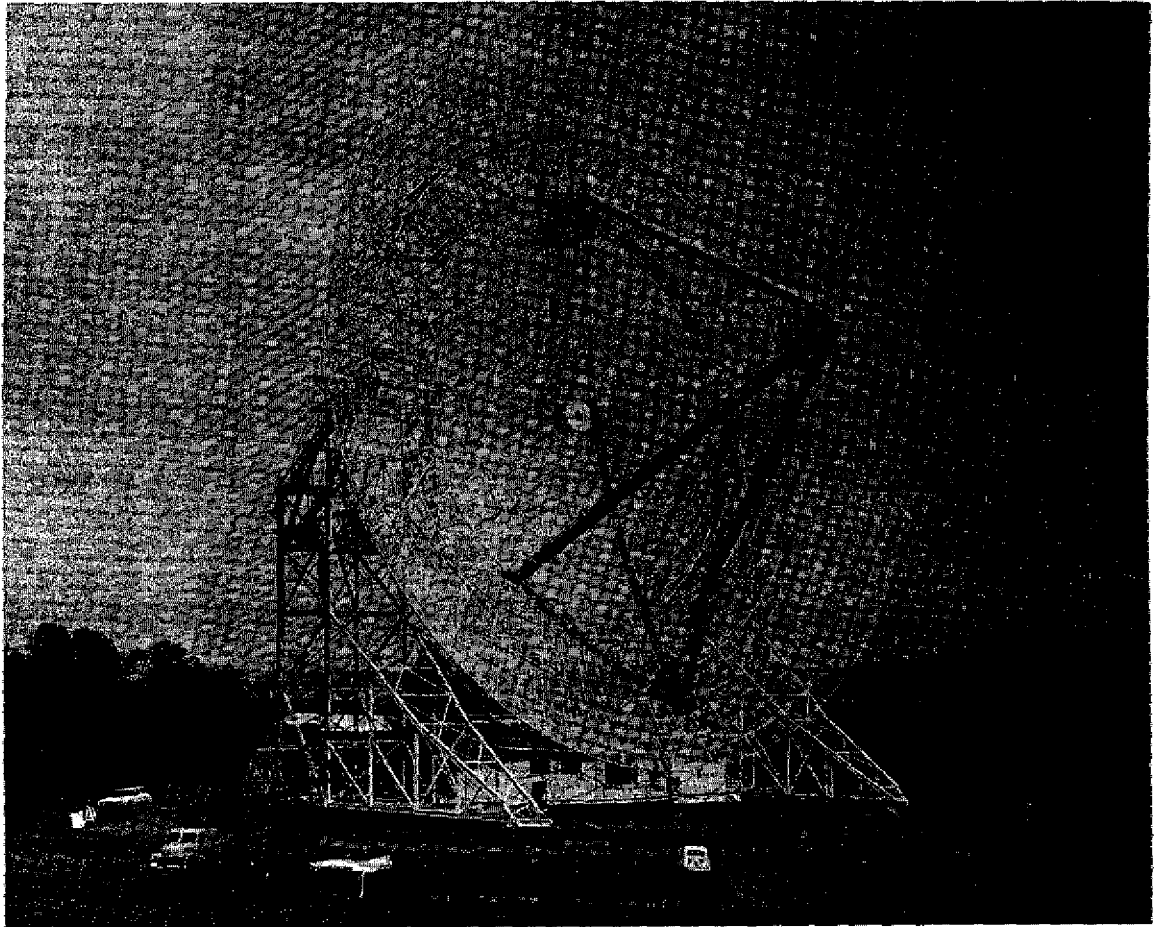


Fig. 1—Randle Cliff Radar

This report describes the most obvious procedure by which one may eliminate the deleterious effect of ground clutter at Randle Cliff without sophisticated computer processing or incorporating extensive antenna or feed redesign or modification. In simple terms, one illuminates the ionosphere in the neighborhood of the horizon, thus extending the effective radar range without (hopefully) extending the range of the ground clutter which is largely limited by earth curvature. In this manner estimates of *E*-region electron densities may be obtained from radar data which are essentially uncontaminated by spurious signals.

The problem of direction finding would appear to be a natural one for which the Thomson scatter technique could be useful as a diagnostic tool. In this connection a set of measurements was initiated in 1970 to assess the ability of a Thomson scatter radar to probe the ionosphere over a highly oblique ray path. One of the first tasks in this investigation was to see if traveling ionospheric disturbances (TID) could be monitored under these conditions. If it proved feasible, then low-elevation Thomson scatter could be used to deduce transverse gradients in electron density, and this knowledge would allow estimates of bearing-angle fluctuations to be made. This report describes some of the measurements of traveling ionospheric disturbances which were made during 1970-71 under low-elevation conditions.

SIMPLIFIED THEORY AND MEASUREMENT TECHNIQUE

A derivation of the formulas which describe the Thomson scattering mechanism would not be relevant for purposes of this report. The interested reader is referred to the voluminous literature which is currently available. For those not theoretically inclined, an excellent review article by Evans (9) will be very helpful in view of its tutorial format.

It will be tacitly assumed at this point that the backscattered power from the ionosphere is governed by the equation

$$P(R) \propto \frac{N(R)}{1 + \beta(R)} R^{-2} \quad (1)$$

where $N(R)$ is the electron density, $\beta(R)$ is the ratio of the electron temperature to the ion temperature, and R is the radar range to the scattering center. This equation is based on the fact that the radar wavelength is much greater than the Debye wavelength in the lower ionosphere. Thus one finds that the backscatter power depends on two quantities which are not necessarily one to one. Since the efficiency of electronic cooling is an increasing function of plasma density, one would expect the larger values of electron content to be associated with the relatively smaller values of β . In fact, a recent study by Dyson et al. (10) suggests that even short-term (wave related) variations in β and N may be out of phase.

Figure 2 is a plot of anticipated backscattered power (with compensation for R^2 spreading and in arbitrary units) for a representative noontime Chapman profile having a scale height of 100 km under zenithal propagation conditions. Two situations are shown: (a) $\beta = 1$ between 100 and 300 km, and (b) β varying between 1 and 3 linearly from 100 to 300 km. Although the situation depicted is highly idealistic, from the point of view of estimating the effect on β on the backscatter power the model selected (b) is not too unreasonable. Taking the lower curve to represent reality, one notes that a discrepancy of $\approx 20\%$ arises by a height of 150 km and at 200 km it is close to 40%. At the $F2$ maximum (taken to be 300 km) the discrepancy is, of course, 100%. Hence one finds that serious error is introduced if one takes $P(R)$ to be proportional to $N(R)$ and ignores the $\beta(R)$ dependence. Faraday rotation obviates the necessity to determine $\beta(R)$ exactly. It is, however, useful to assume that it is slowly varying. That is, $\beta(R)$ will be required to exhibit spatial variations which are not more rapid than those belonging to $N(R)$.

The amount of Faraday rotation exhibited by linearly polarized radio waves over a two-way path is given by

$$\Omega(R) = 5.95 \times 10^{-2} f^{-2} \int_0^R H(R') \cos \theta(R') N(R') dR', \quad (2)$$

where f is the radar frequency, $H(R')$ is the magnetic field intensity in ampere turns/meter, θ is the angle between the ray trajectory and magnetic field vector, and Ω is the Faraday-rotation angle in radians.

Employing linear polarization and taking Faraday rotation into account, one finds that Eq. (1) for the backscatter power should be modified to read

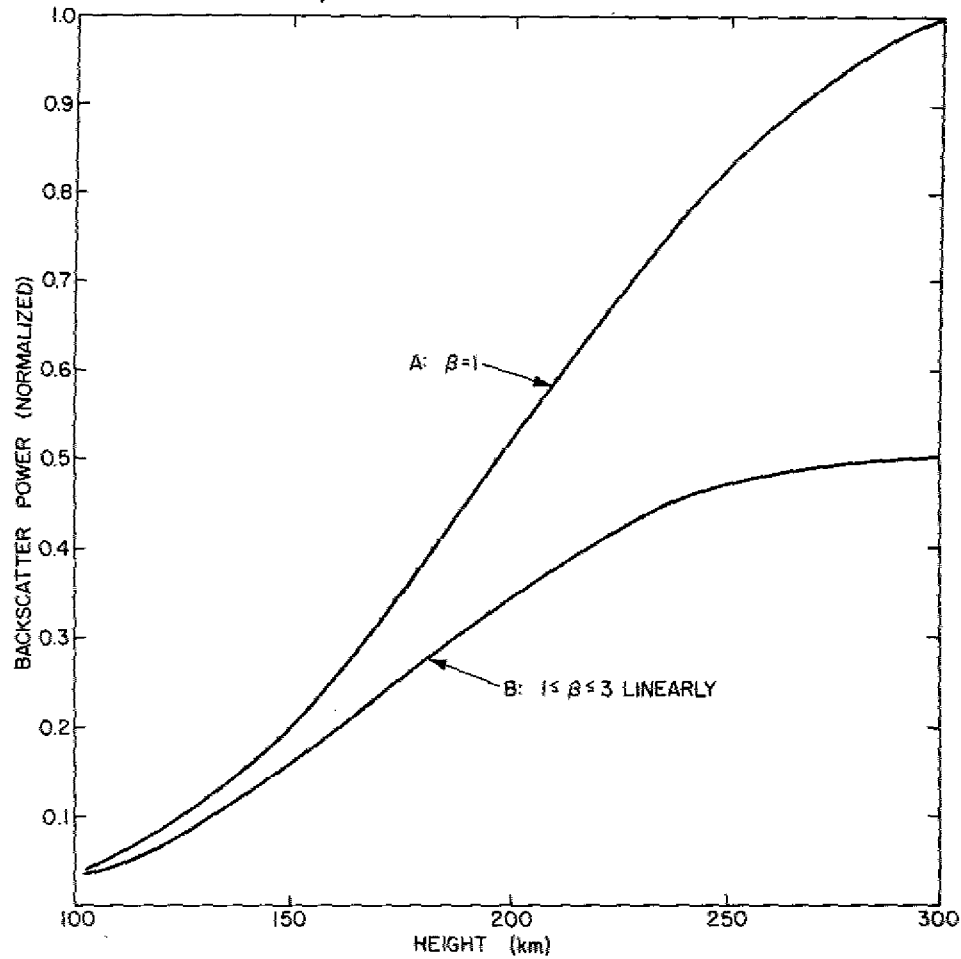


Fig. 2—Backscatter power as a function of ionospheric height. A Chapman electron-density profile having a scale height of 100 km and an $F2$ maximum height of 300 km is assumed. Two situations are considered for illustrative purposes: Curve A (solid) is the predicted power under the assumption that $\beta = 1$ for all heights, and curve B (dashed) is the predicted power for β varying from 1 to 3 linearly between 100 and 300 km in height.

$$P(R) \propto R^{-2} \left[\frac{N(R)}{1 + \beta(R)} \right] \left[\begin{matrix} \sin \\ \cos \end{matrix} \Omega(R) \right]^2. \quad (3)$$

Provided that the receiver detector is operating in the linear region and that the signal-to-noise ratio is small ($S/N \ll 1$), the measured voltage $V(R)$ is proportional to the backscatter power. That is, the linear detector acts like a square-law device for low S/N . This point is discussed by Evans (11). In Eq. (3) the cosine is taken if the transmitted polarization is received, and the sine is taken if the orthogonal polarization is received. Clearly if the linear polarization is used and polarization of the scattered wave remains discernible, one would expect to see a rather "wiggly" backscatter power profile. The envelope of this profile is proportional to the term $N(R)/[1 + \beta(R)]$, but the modulation rate is proportional to $N(R)$ alone. One would hope that $N(R)R^{-2}/1 + \beta(R)$ does not vary significantly during the modulation period associated with $\Omega(R)$. One finds, however, that this is an unreasonable hope except near the $F2$ maximum. Nevertheless, provided the variation is smooth, it is still possible to estimate $\Omega(R)$ strictly from an amplitude analysis with predictable error.

Calling $H \cos \theta = \psi^*$ for short (the star used to distinguish it from $\psi = H \cos \theta \sec \chi$, where χ is the ray zenith angle), one deduces the following simple expression for the electron density:

$$N(R) = \frac{16.8 f^2}{\psi^*(R)} \frac{d\Omega(R)}{dR}. \quad (4)$$

The only unknown in Eq. (4) is the derivative of Ω , since ψ^* is completely specified by the experimental geometry. This function has been discussed in earlier work, e.g., Ref. 12. Figure 3 depicts the variation of ψ^* for several selected ray trajectories launched from Randle Cliff.

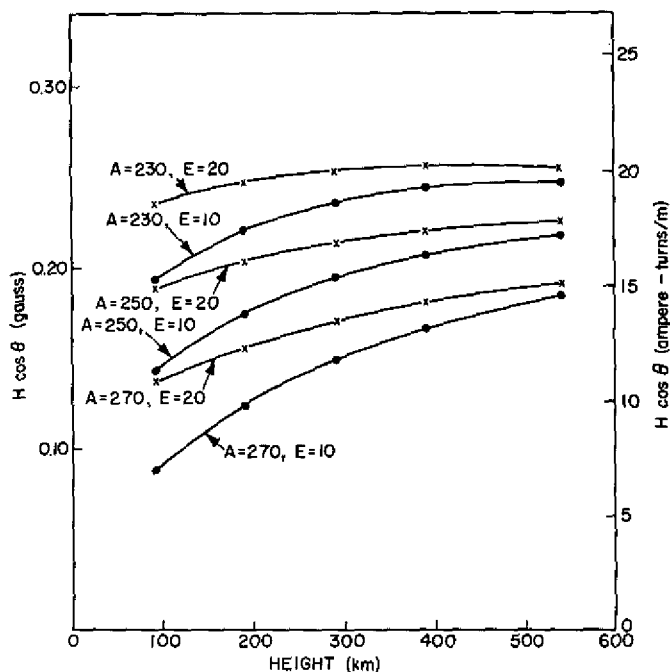


Fig. 3—Variation of $\psi^* = H \cos \theta$ for several ray trajectories

FARADAY DISPERSION

In some instances, especially whenever the pulse length is quite long, Faraday dispersion may destroy the ability to measure Ω near the $F2$ maximum. (The problem of dispersion has been discussed by Farley (4) and has been shown by Goodman (13) to be useful as an alternative procedure for deducing electron-density profiles.) It turns out that Faraday dispersion is one of the more troublesome aspects of the low-elevation-angle studies undertaken at Randle Cliff. This is because at low elevation the use of a relatively large pulse length τ is required to increase the signal-to-noise ratio, and Faraday dispersion is roughly proportional to τ . Hence it is often impossible to measure Faraday rotation near the $F2$ maximum where N is large and Ω is changing rapidly. It is also remarked that a distinctly different type of Faraday dispersion appears in low-elevation experiments. It is called beamwidth dispersion and is irreducible as far as the pulse length is concerned.

Figure 4 illustrates the effect of dispersion for pulse lengths of 25, 50, 100, and 200 μs . Although these curves do not refer to the low-elevation geometry, it is clear that a substantial pulse length will render the Faraday rotation data almost irretrievable.

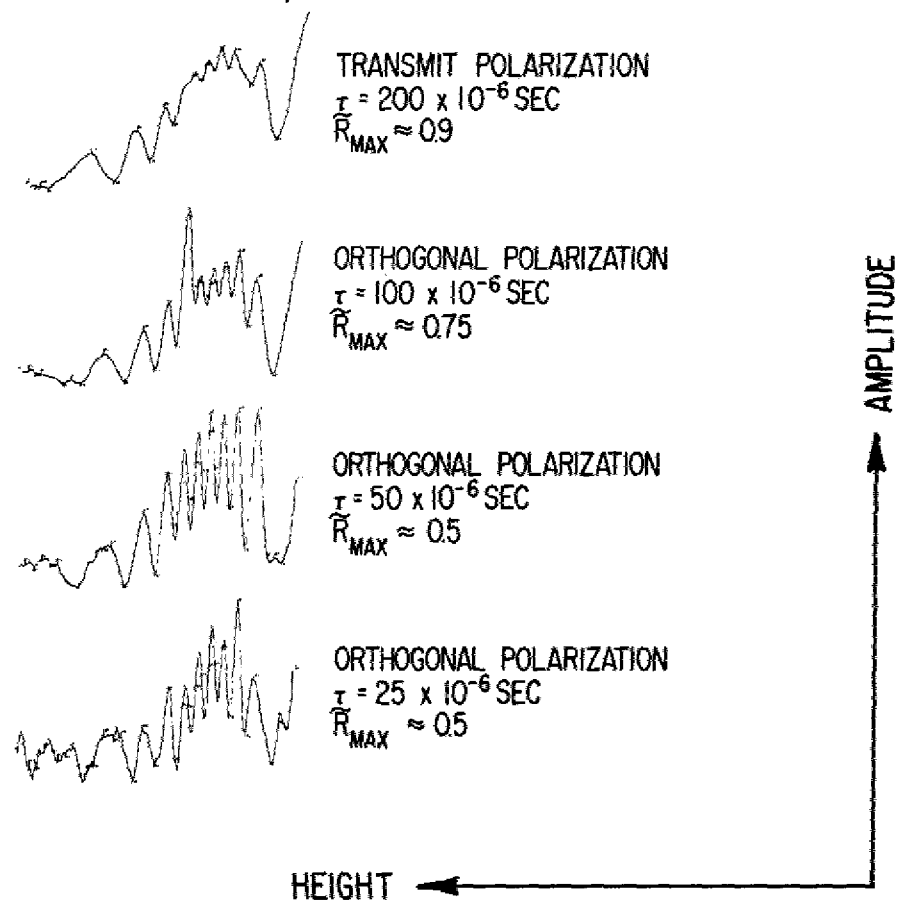


Fig. 4—Faraday-rotation profiles of the backscatter power obtained using pulse lengths of 25, 50, 100, and 200 μs . \bar{R} is the ratio of a particular minimum to the average of its neighboring maxima. \bar{R}_{max} is the greatest of these ratios.

Furthermore, for depressed elevation angles the situation will be even worse, since beam-width dispersion and horizontal gradient effects cannot be neglected. Practically speaking, the pulse length is limited probably to about 200 μs as far as the Faraday rotation measurements are concerned, and this value for τ gives a coverage of between roughly 100 and 300 km. This is presumably adequate for present purposes.

INITIAL BACKSCATTER PROFILES

To determine the feasibility of obtaining electron-density profiles over a highly oblique radar path, an initial test was conducted on March 27, 1970. In this test linear and circular polarizations were employed alternately. Elevation angles of 10, 15, and 20 deg were each used at azimuth positions of 240, 243, and 246 deg. Figure 5 illustrates the effect on the backscatter profile of changing the elevation using circular polarization. One can note that the base of the E region (taken to be close to 100 km) is much better defined at 10 deg than at either 15 or 20 deg. Due to the pulse length employed in these tests (500 μs), Faraday dispersion was a serious problem when transmitting and receiving linear polarization. Figure 6 shows three profiles, the first and last based on linear-polarization data and the second extracted from circular-polarization data. By measuring

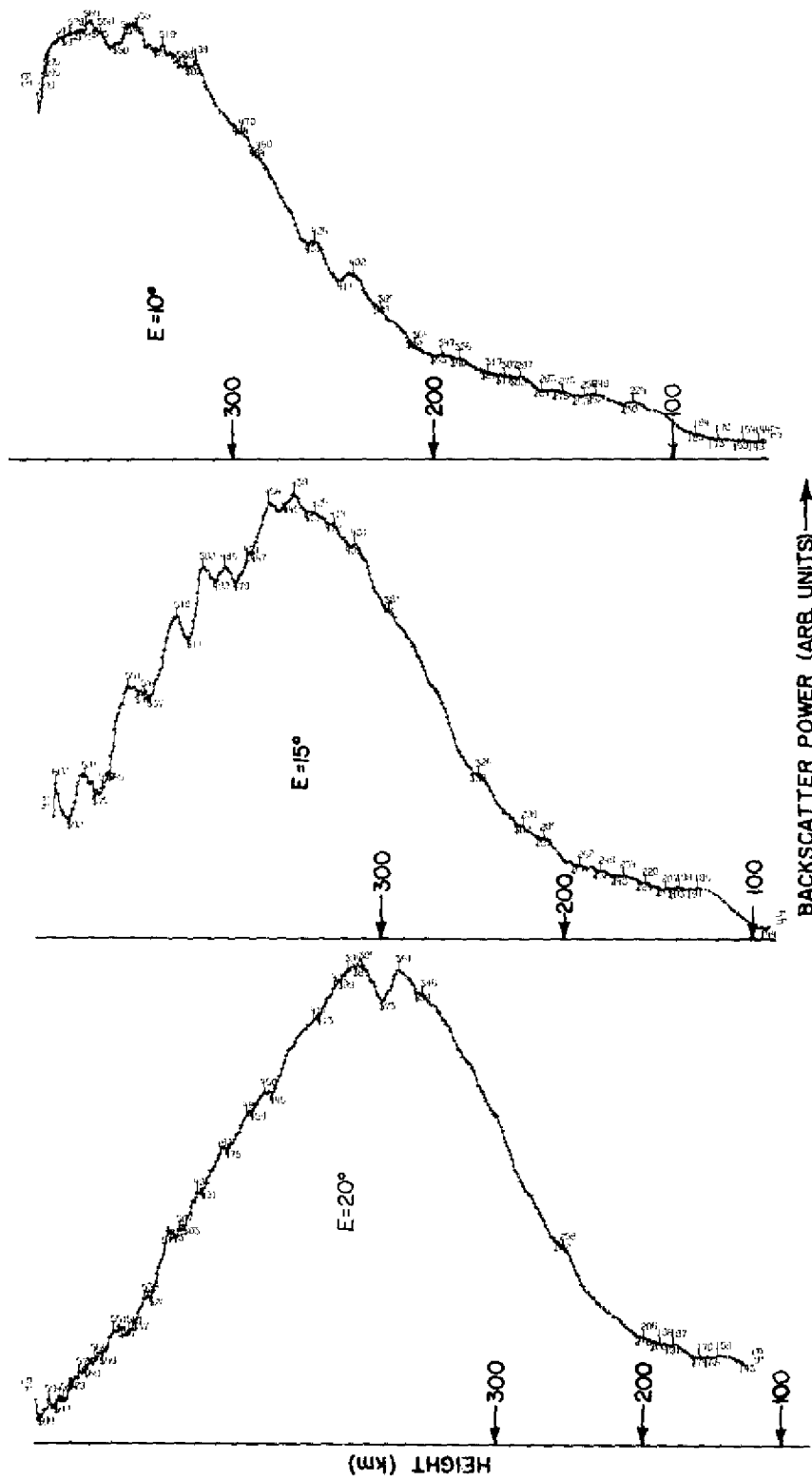


Fig. 5—Changes in the backscatter power profile resulting from elevation-angle differences

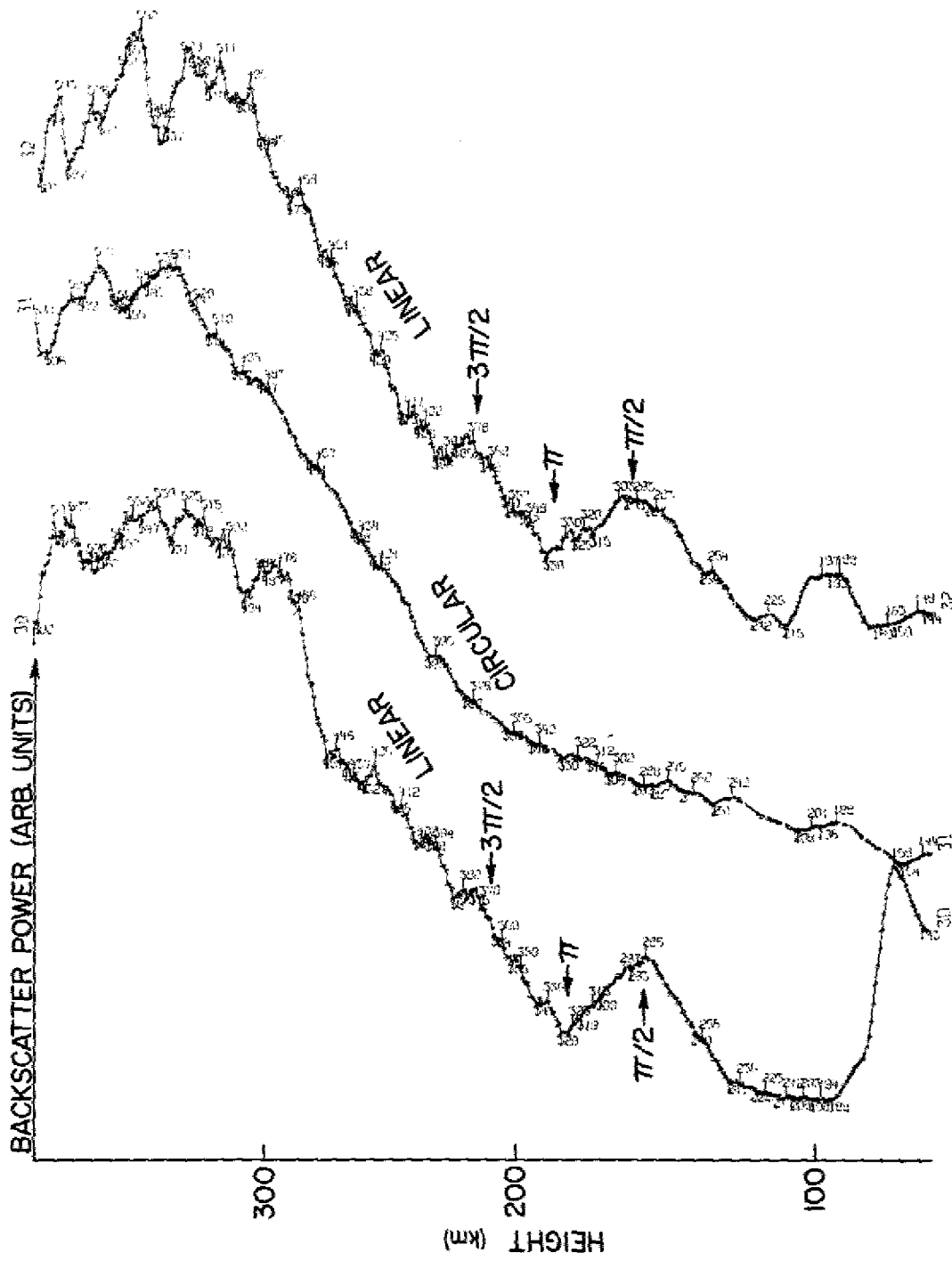


Fig. 6—Comparison of linear and circular-polarization data. Daytime profiles are shown.

the derivative $d\Omega/dR \approx (\pi/2)/\Delta R$ at some point[†] and by applying the appropriate ψ^* factor, it is possible to calibrate the power profile under the assumption that $\beta(R) = 1$. Two facts serve to produce errors in this calibration procedure. First, the value of electron density deduced from the Faraday rotation data is an average over a range interval ΔR , and this average is assumed to characterize the midpoint of the range interval. This is not justifiable unless $N(R)$ is roughly linear over ΔR . Second, β may safely be assumed to be unity below a height of 120 km but not above. As indicated by Fig. 2, there is an estimated discrepancy of 15-20% at 150 km between the true $N(h)$ profile and the profile neglecting $\beta(R)$. Assuming that $\beta(R) = 1$ at 120 km rather than at 100 km, the discrepancy ranges between 10% and 15%. The proper procedure to be followed for measurements at low elevation should consist of a series of runs for which linear and circular polarization are employed alternately. However, a short pulse length of $\approx 100 \mu s$ should be used for the Faraday rotation runs to reduce the dispersion problem and thus expose more Faraday extrema. In this fashion a skeleton $N(R)$ profile—call it $N_s(R)$ —may be computed from the linear polarization data, and a comparison of this profile with the (circular polarization) power profiles will yield $\beta(R)$. One may recall that

$$P(R) = K \left[\frac{1}{1 + \beta(R)} \right] N(R) R^{-2} \quad (5)$$

where K is a calibration factor to be evaluated where $\beta(R) = 1$. Thus by comparing the power measurement at R_0 with the estimate of N_s there,

$$K = \frac{2P(R_0)R_0^2}{N_s(R_0)}, \quad (6)$$

which is true provided R_0 (parameterized in terms of height h) is less than $R(h = 120 \text{ km})$. One defines $\beta(R)$ as

$$\beta(R) = \left[\frac{KN_s(R)R^{-2}}{P(R)} - 1 \right]. \quad (7)$$

Therefore using this skeleton electron-density profile and this estimate of K at R_0 , a $\beta(R)$ function has been constructed. This function is then used together with power profiles to deduce a more refined electron-density distribution $N(R)$. This approach was not followed during the series of tests reported in this report. All data thus far analyzed were obtained by employing linear polarization only; as a consequence, only skeleton profiles have been deduced.

In retrospect, this might appear to be an error in judgment; however, experience in interpreting Faraday rotation data had been firmly established by the time the tests were initiated, whereas the treatment of the power profiles was not established. Furthermore, time resolution was presumably a factor owing to the existence of short-period (≈ 20 min) traveling ionospheric disturbances whose detection was sought. By conducting both circular- and linear-polarization runs alternately, the time resolution would have been degraded by a factor of two. This would have been serious, since the basic running time is ≈ 5 min, which suggests that ≈ 10 min would separate independent samples. As a result,

[†]The derivative of the Faraday-rotation angle is deduced by finding the range interval ΔR over which a rotation of $\pi/2$ (or 90 deg) occurs. This distance is just the range separation between adjacent extrema.

a 20-min TID could only barely be resolved. The sampling situation was further complicated by the fact that some azimuthal scanning was desired to deduce transverse gradients in electron density. On considering the possible analytical problems which would have been encountered as well as the possible loss in temporal resolution, the decision to forego the acquisition of circular polarization data was certainly proper.

Hereafter all electron-density values, though based on skeleton determinations and denoted by N_s in the present section, will be denoted by the term N .

SEARCH FOR TRAVELING IONOSPHERIC DISTURBANCES

Table 2 lists the low-elevation experiments which have been conducted to date. Approximately 102 hr of radar operation are represented by the series of tests which are tabulated. Most of the data correspond to linear modes of transmission and reception; only three tests were conducted for which circular polarization was available. However, this was deliberate, so as to take advantage of the Faraday effect. In addition, only a single polarization channel was received in most instances (denoted by the symbol A), and this channel was orthogonal to the so-called transmit polarization (denoted by the symbol B). The tabular designation for reception of two orthogonal polarization modes is AB .

Table 2
Low-Elevation Thomson Scatter Experiments

Date	Reel	File	Data Mode	Polarization	Time	Azimuth (deg)	Elevation (deg)
Mar. 26, 1970	52	83	← Test →				
Mar. 27, 1970	52	84	← Test →				
Apr. 14, 1970	58	90	A	Linear	0950-1520 EST	240/243/246	20
May 19, 1970	70	102	A	Linear	1530-2020 EST	242	10
May 21, 1970	71	103	A	Linear	1530-2010 EST	240/245	15
May 27, 1970	76	108	A	Linear	0400-0850 EST	240/245	15
Jun. 24, 1970	91	123	A	Linear	0430-0800 EST	232/242/252	15
Jun. 25, 1970	92	124	A	Linear	0945-1335 EST	232/242/252	15
Jul. 1, 1970	93	125	A	Linear	0900-1400 EST	232/242/252	15
Aug. 11, 1970	102	137	AB → 1940 A → 2100	Linear → 1940 Circular → 2100	1525-2100 EDT	232/252	15
Aug. 12, 1970	103	138	AB	Linear	1005-1515 EDT	242	15
Aug. 13, 1970	104	139	AB	Linear	1000-1455 EDT	242	15
Aug. 14, 1970	105	140	A	Circular	0600-1005 EDT	232/252	15
Sep. 22, 1970	125	163	A	Linear	0700-1800 EST	246/263	12
					1800-1930 EST	253	
Oct. 23, 1970	130	168	A	Circular	0800-1224 EST	250/270	15
Oct. 27, 1970	131	169	A	Linear	1330-1558 EST	243	15
Oct. 28, 1970	132	170	A	Linear	1020-1515 EST	243	15
Feb. 23, 1971	137	175	A	Linear	1000-1550 EST	243	15
Feb. 24, 1971	138	176	A	Linear	0720-1500 EST	243	15
Feb. 26, 1971	139	177	A	Linear	0820-1610 EST	233	15
Mar. 3, 1971	141	183	A	Linear	1124-1625 EST	232	15

Skeleton Electron Density Profiles

Two techniques have been employed for the determination of skeleton $N(R)$ profiles with the distinguishing feature being the procedure by which the derivative dN/dR is formed. The first technique (referred to as 1) is to smooth the Faraday-rotation function

$\Omega(R)$ by fitting the raw rotation-angle data to a least-square polynomial which is differentiated analytically. This is justifiable, since the estimates of Ω are rather noisy in most cases. This derivative is naturally continuous, and hence one obtains a continuous function $N(R)$ on application of equation (4). Figures 7-9 are plots of the smoothed $\Omega(R)$ functions as well as the derived $N(R)$ profiles for Aug. 11-13, 1970. A height scale is also indicated on each run. In these three cases a fourth-degree polynomial is used to fit the $\Omega(R)$ data.

The second technique (referred to as 2) for deducing $N(R)$ profiles involves a more direct computation of N by forming the average derivative and using the result in Eq. (4). The average derivative is computed between adjacent extrema by means of the relation

$$\left\langle \frac{d\Omega(R)}{dR} \right\rangle \approx \frac{\pi/2}{\Delta R} \quad (8)$$

where ΔR is the range separation between rotation angles of $m\pi/2$ and $(m+1)\pi/2$, $m = 0, 1, 2, \dots$. This procedure suggests that one estimate of N can be extracted for each 90 deg of rotation, two estimates per Faraday fade, or four estimates per complete rotation. (Quite naturally, if the ionosphere becomes markedly tenuous, then one would expect to obtain a meager number of electron-density estimates. For this reason one would not generally attempt to use the Faraday method during nocturnal hours. Also, late in the evening there is some justification in assuming $\beta = 1$, so that in that instance there is an unequivocal relationship between $N(R)$ and the backscatter power $P(R)$.)

The values of N obtained by this procedure are plotted at the midpoint of the range interval ΔR over which N applies. The next step is to fit these data to a least-square polynomial to obtain a continuous function $N(R)$. Figures 10-16 illustrate the results of this procedure.

Figures 7-9 and 12-14 are particularly interesting since they refer to August 11-13, 1970. Comparing the August results obtained by methods 1 and 2, one notes that there are substantial differences. In particular, one finds that the $F2$ maximum density is consistently underestimated by technique 1. This is especially noticeable in the case of August 11. Due to the scatter of the data points, it is difficult to choose between the two techniques above the $F2$ maximum. Nevertheless, it would appear that technique 1 is in closer agreement with the actual data in that region. Below the $F2$ maximum it is clear that technique 2 is a better fit to the data points.

Faraday Rotation Isopleths

Figure 17 is an example of a set of Faraday rotational isopleths obtained on May 19, 1970. Data were obtained at an elevation angle of 10 deg and an azimuth angle of 242 deg. One can note a wave-like disturbance having a period of roughly 15 to 20 min. Such wave-like features are thought to be associated with neutral gravity waves which have a lower limiting period to ≈ 10 min in the lower thermosphere (Vaisala-Brunt period).

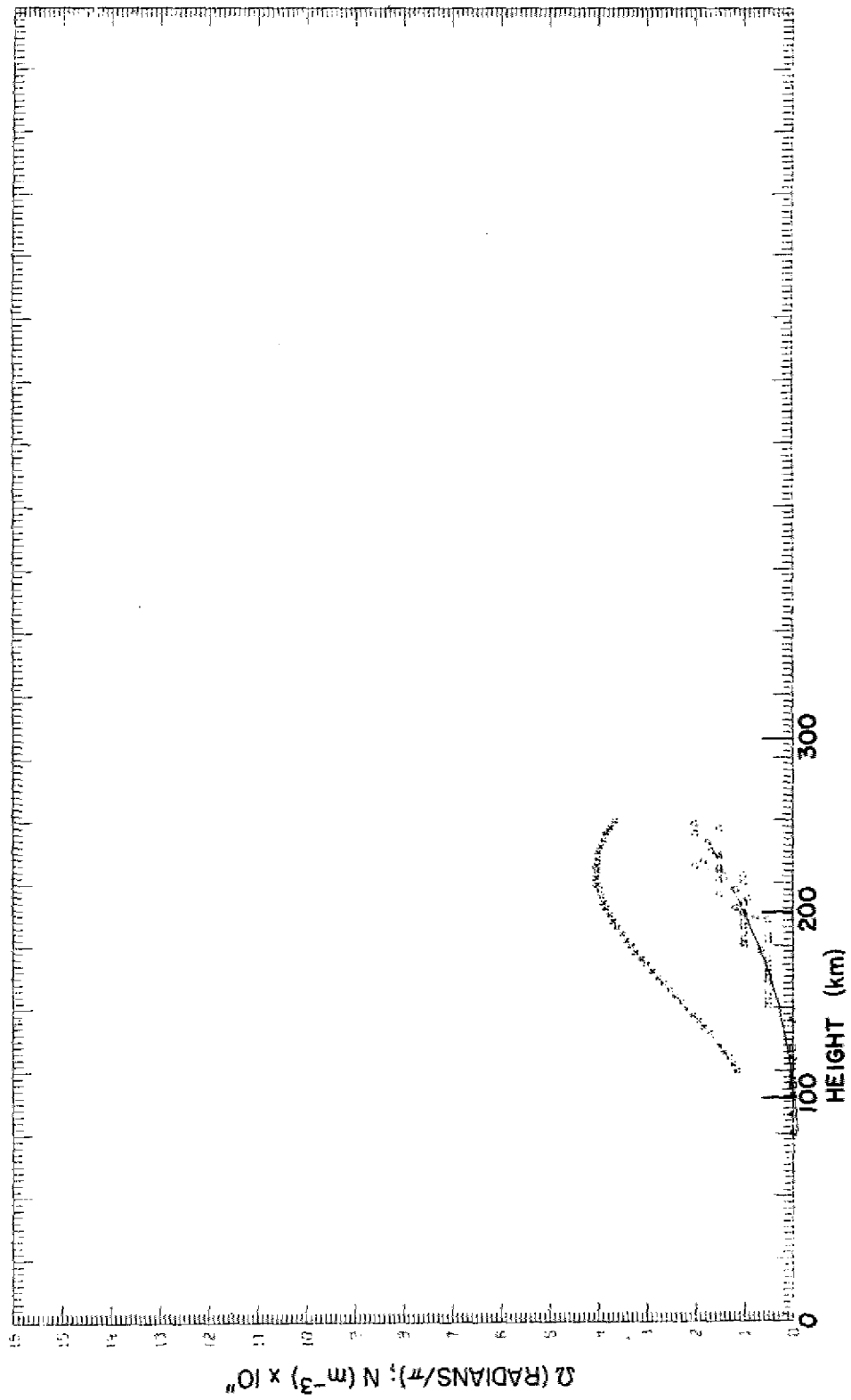


Fig. 7—Electron-density distribution obtained on Aug. 11, 1970, 1425-1840 EST using method 1. The Ω data (squares) were fitted to a fourth-degree polynomial.

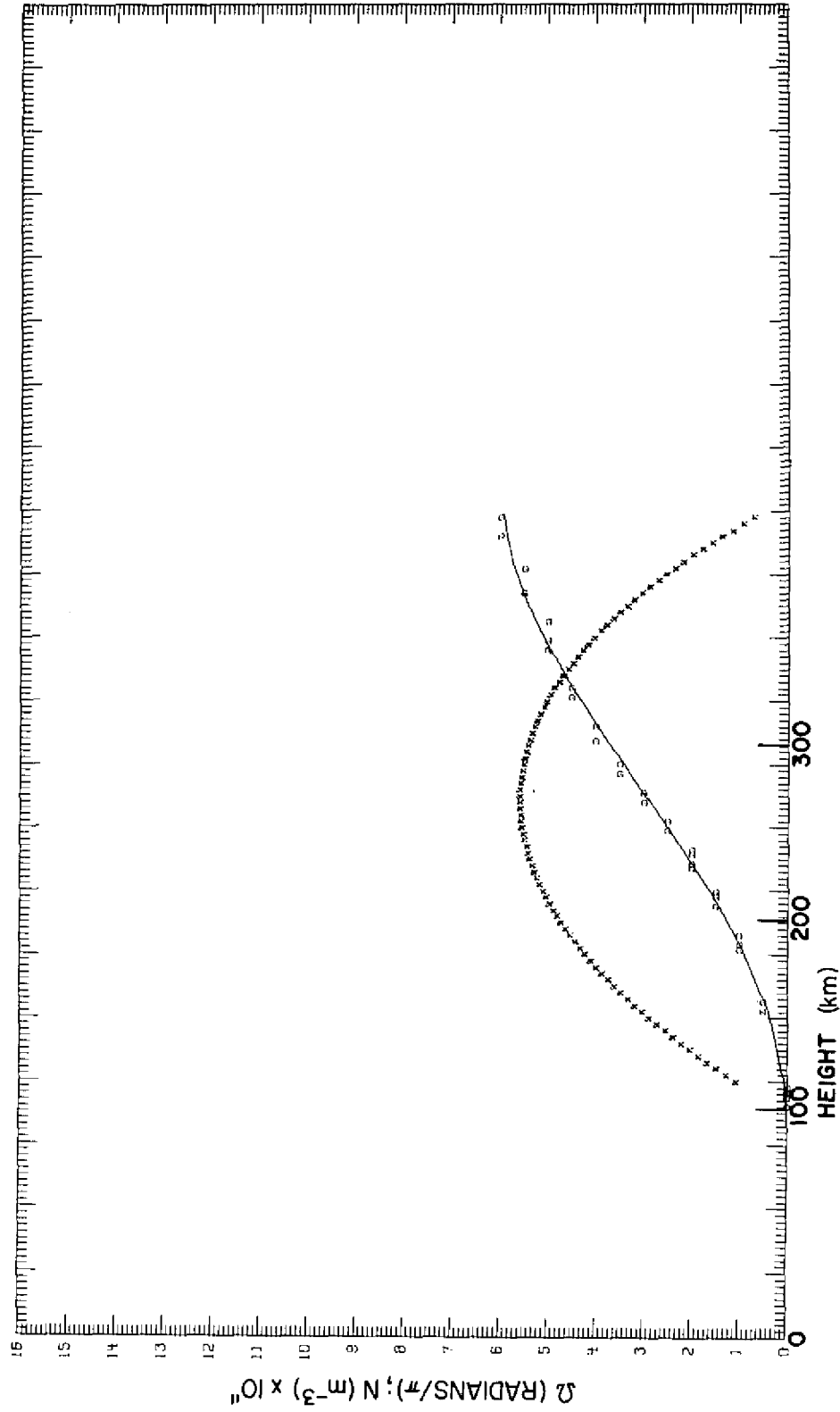


Fig. 8—Electron-density distribution obtained on Aug. 12, 1970, 0905-1415 EST using method 1. The Ω data (squares) were fitted to a fourth-degree polynomial.

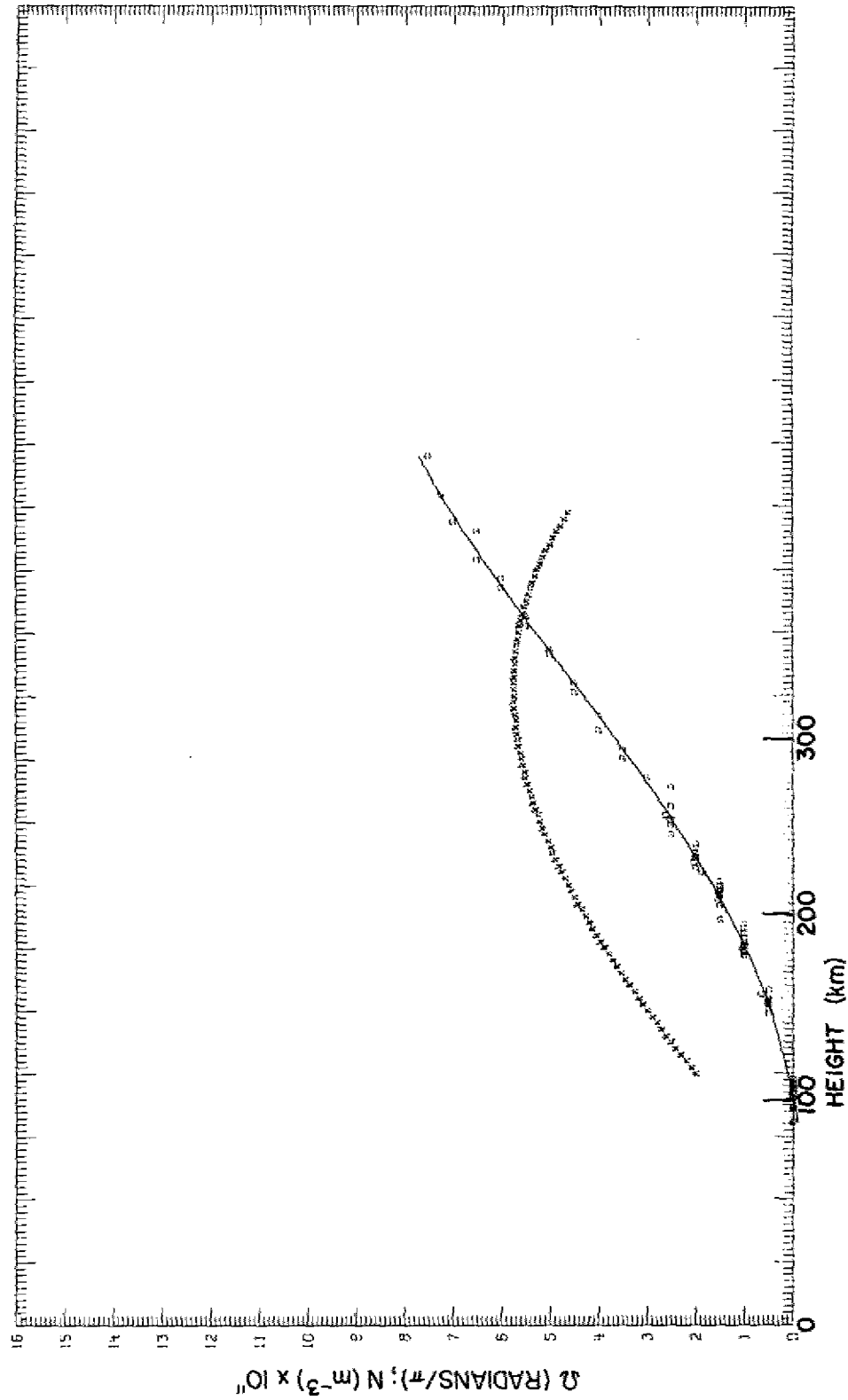


Fig. 9--Electron-density distribution obtained on Aug. 13, 1970, 0900-1355 EST using method 1. The Ω data (squares) were fitted to a fourth-degree polynomial.

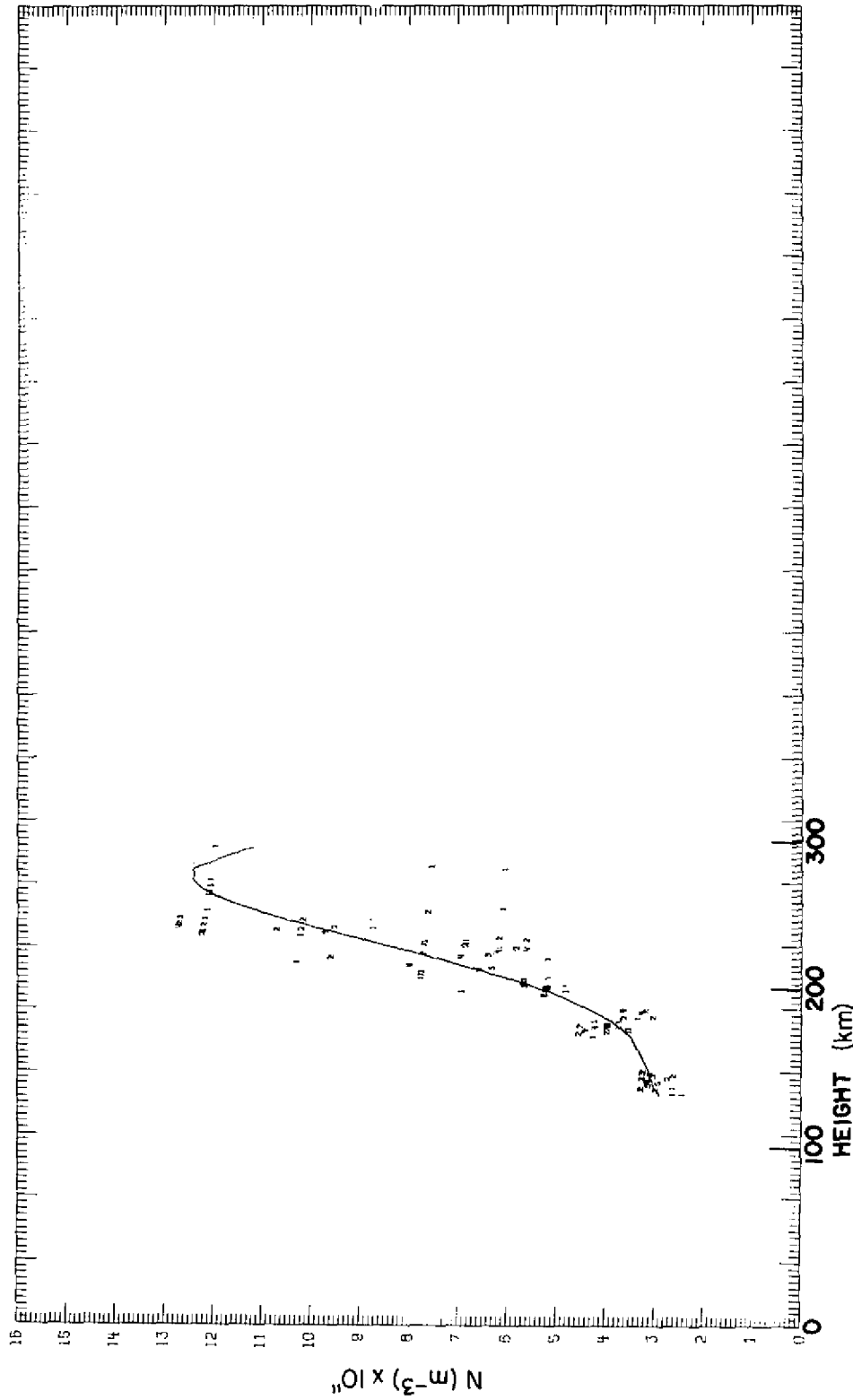


Fig. 10—Electron-density distribution obtained on Apr. 14, 1970, 0950-1520 EST using method 2. The individual estimates of N are fit to a fourth-degree polynomial.

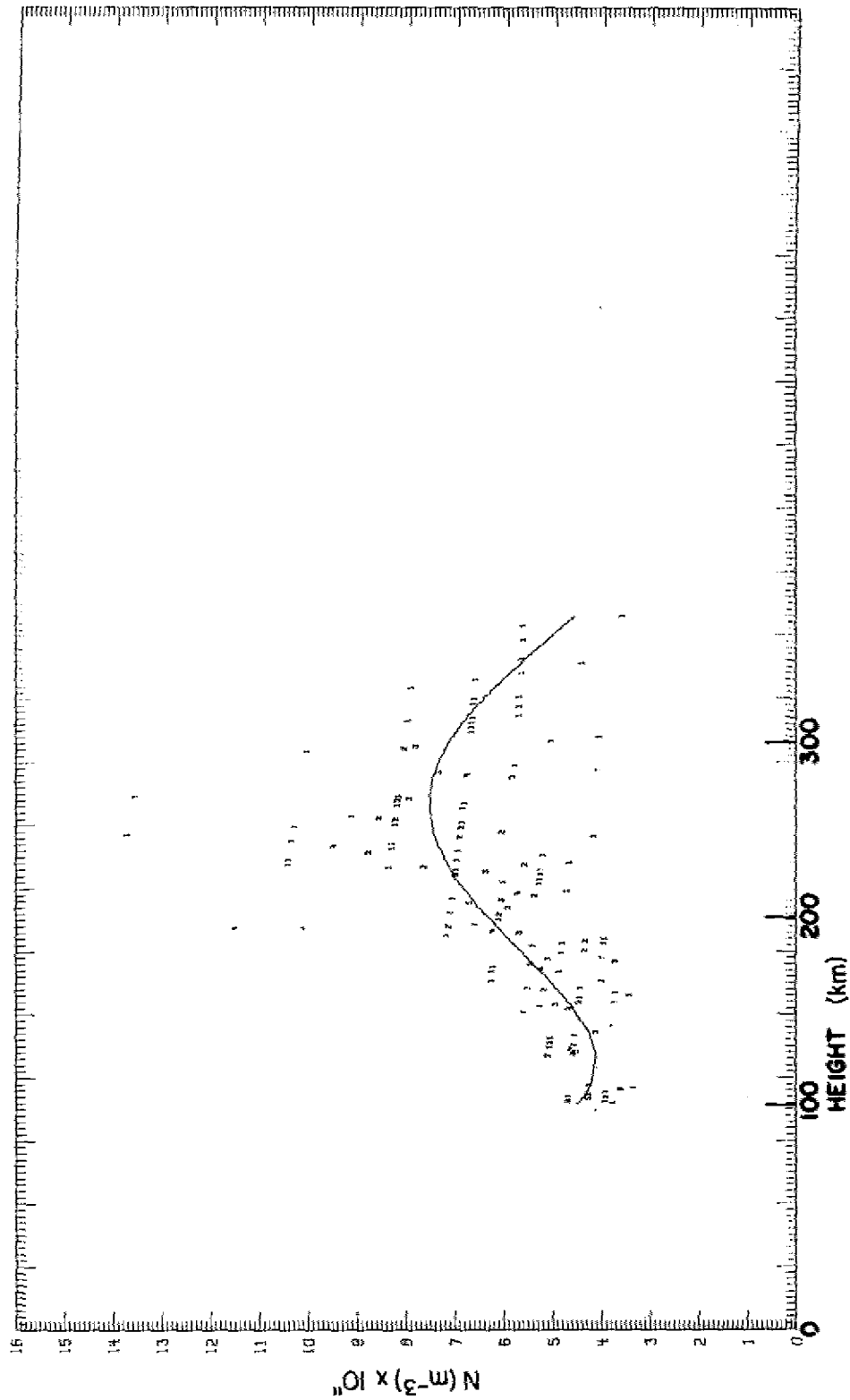


Fig. 11 — Electron-density distribution obtained on July 1, 1970, 0900-1400 EST using method 2. The individual estimates of N are fit to a fourth-degree polynomial.

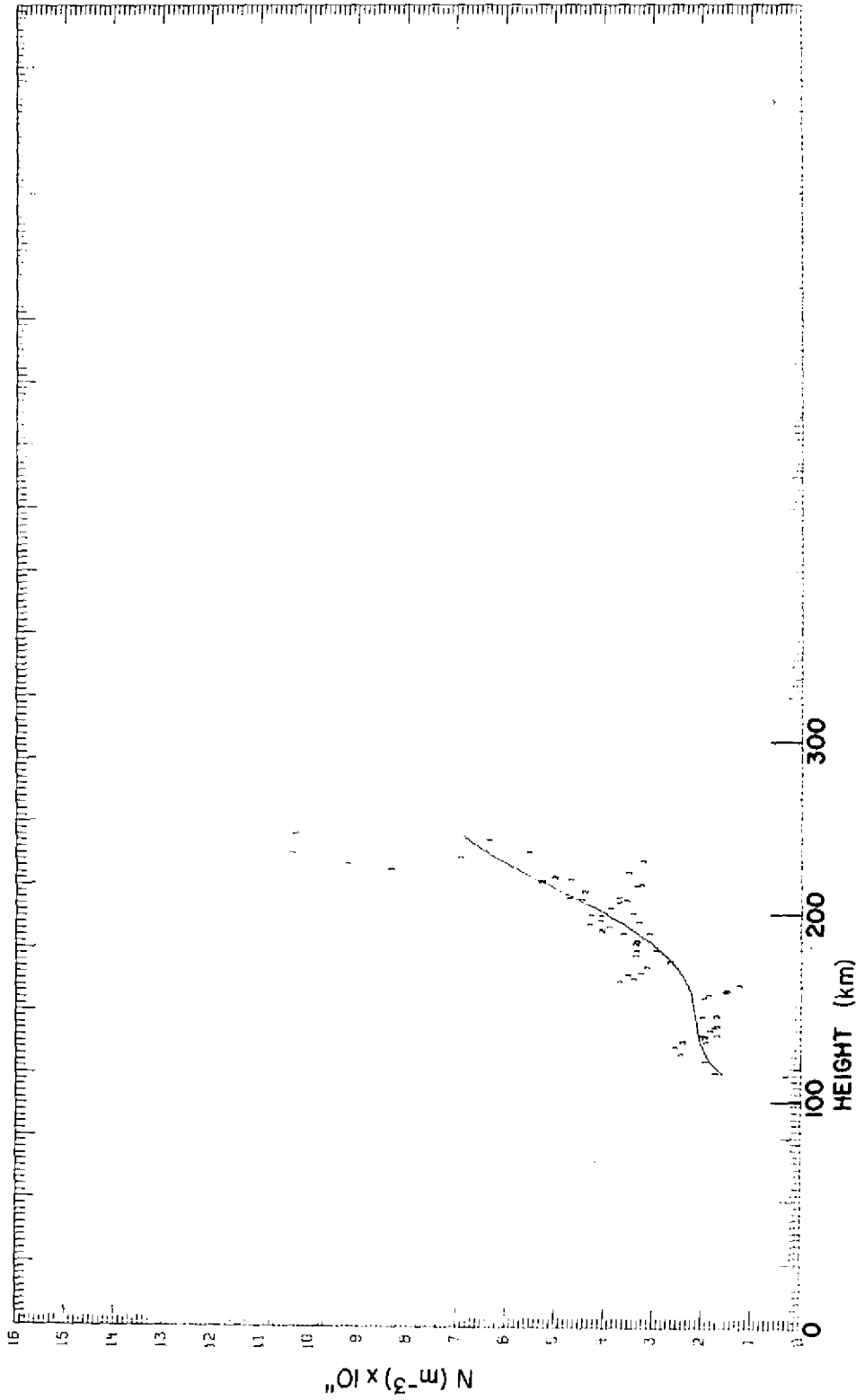


Fig. 1.2—Electron-density distribution obtained on Aug. 11, 1970, 1425-1840 EST using method 2. The individual estimates of N are fit to a fourth-degree polynomial.

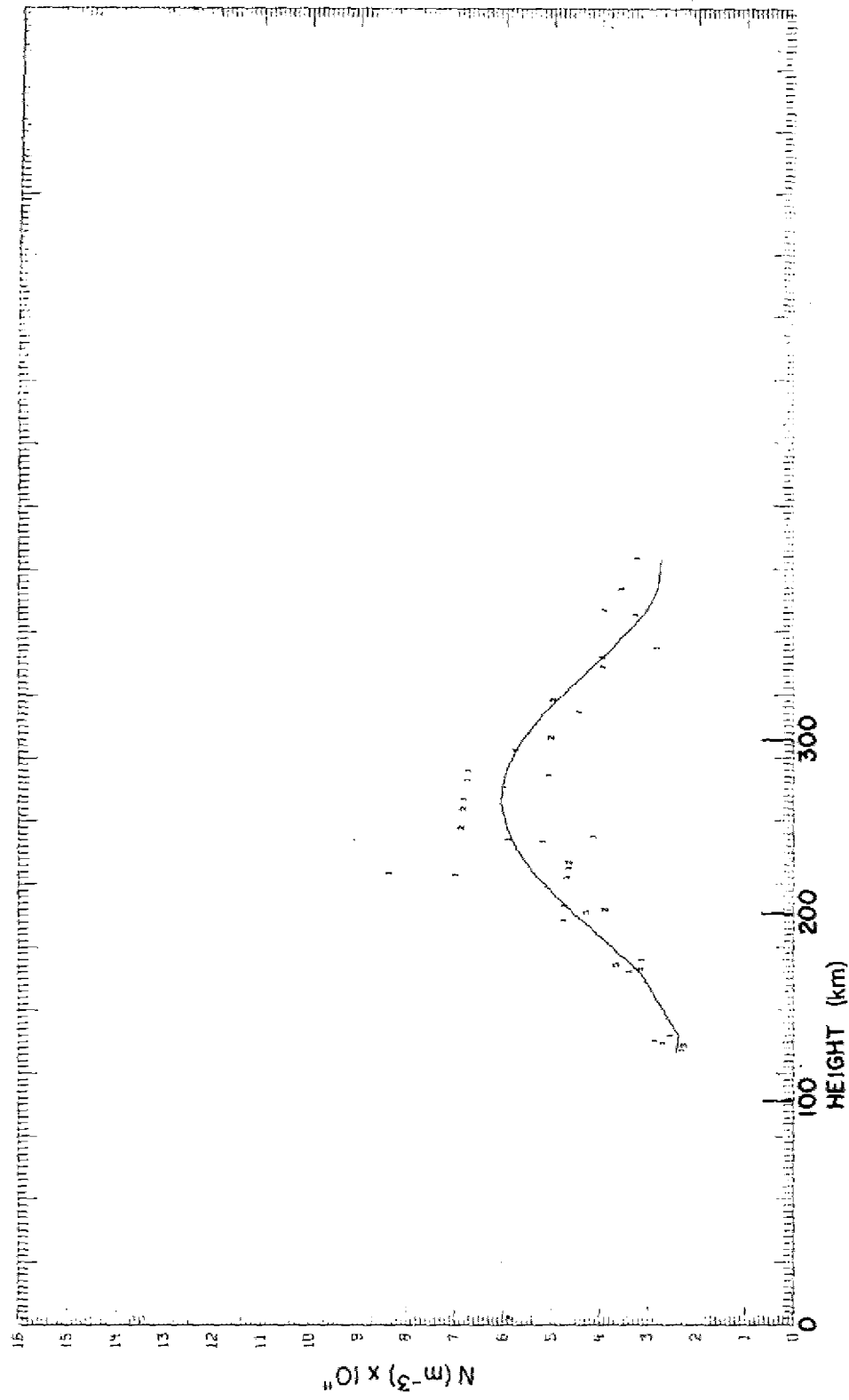


Fig. 13—Electron-density distribution obtained on Aug. 12, 1970, 0905-1405 EST using method 2. The individual estimates of N are fit to a fourth-degree polynomial.

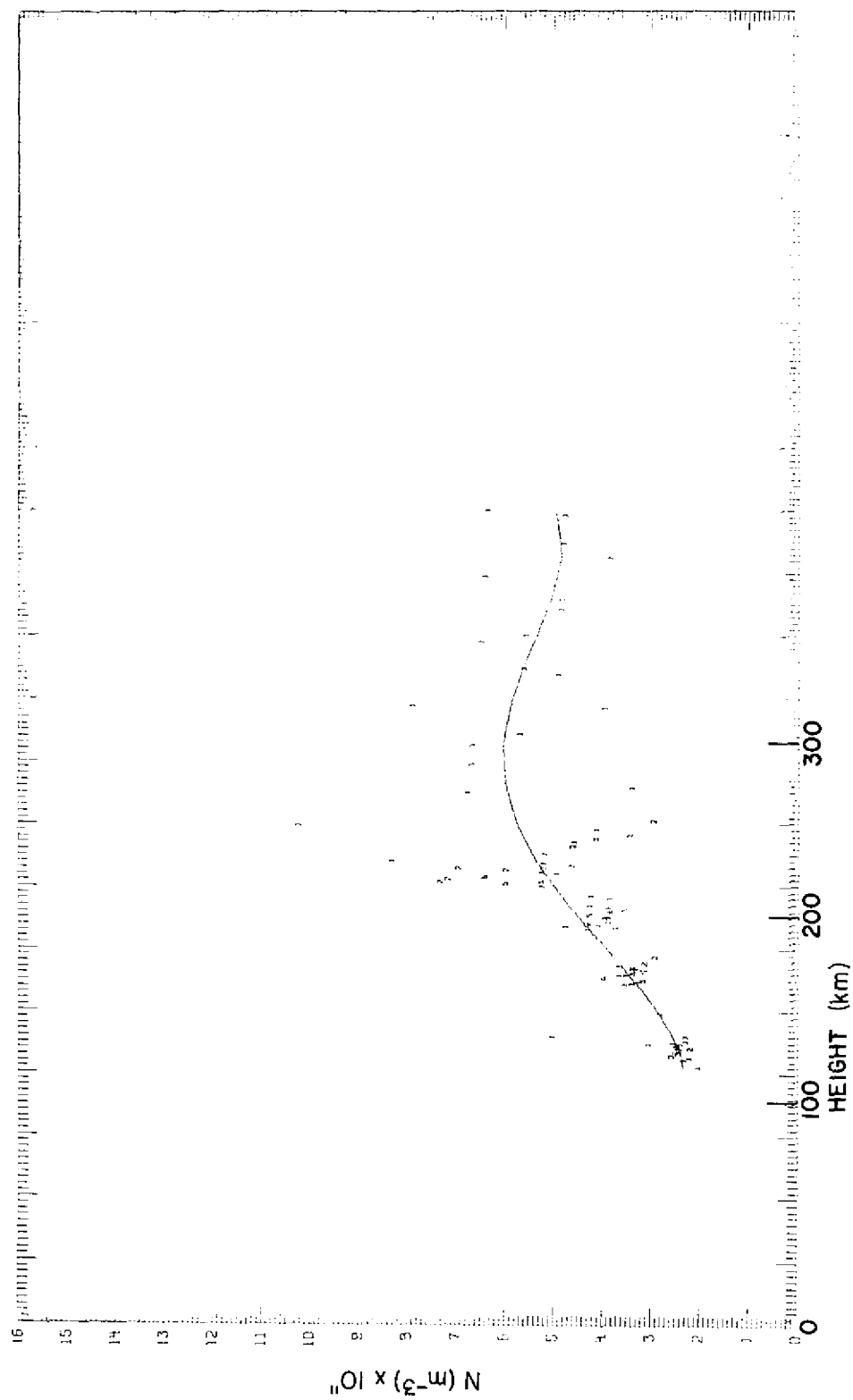


Fig. 14—Electron-density distribution obtained on Aug. 13, 1970, 0900-1355 EST using method 2. The individual estimates of N are fit to a fourth-degree polynomial.

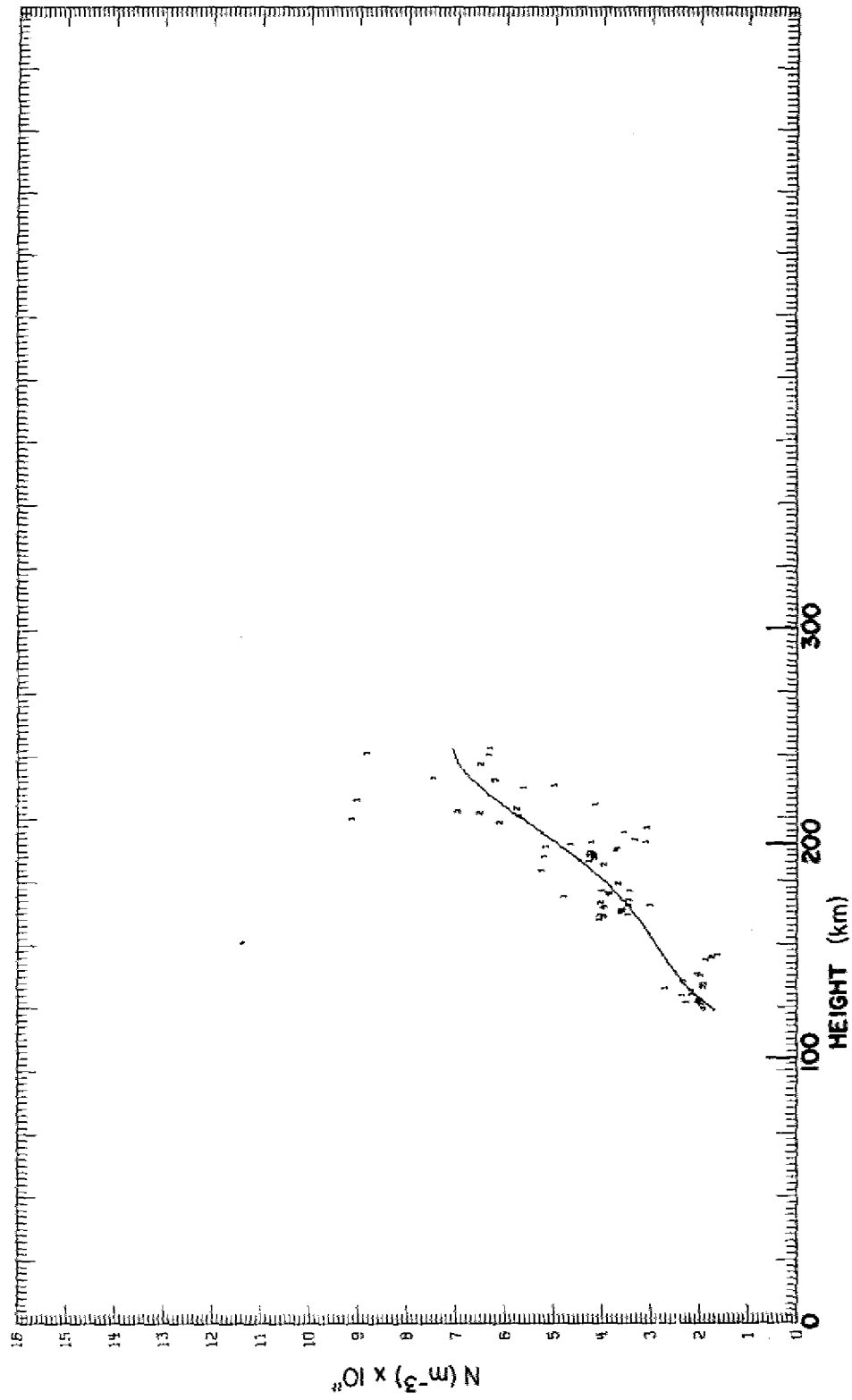


Fig. 15--Electron-density distribution obtained on Sept. 22, 1970, 0700-1800 EST using method 2. The individual estimates of N are fit to a fourth-degree polynomial. The radar was pointed toward the general direction of San Antonio, Texas.

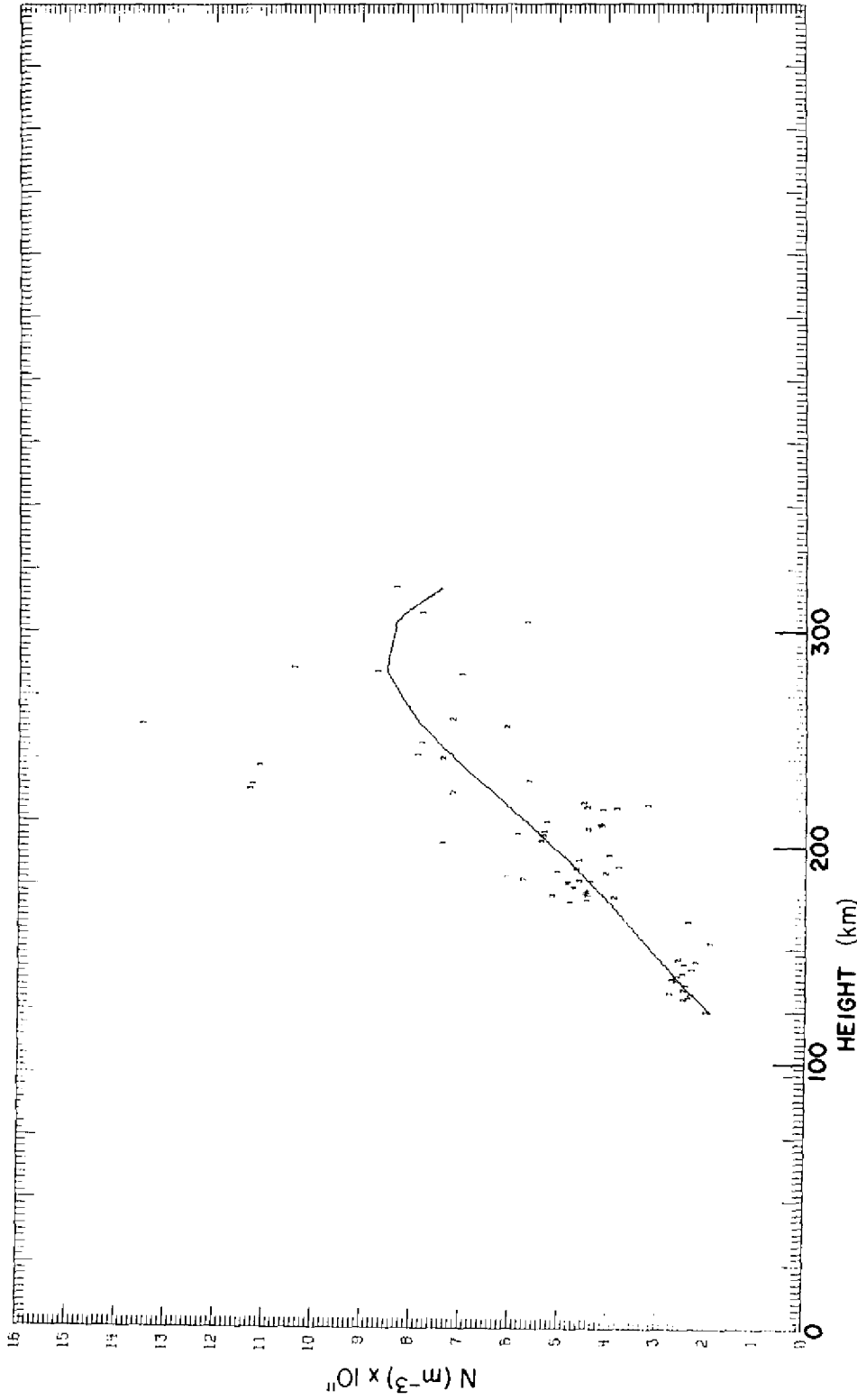


Fig. 16—Electron-density distribution obtained on Sept. 22, 1970, 0700-1800 EST using method 2. The individual estimates of N are fit to a fourth-degree polynomial. The radar was pointed toward Lubbock, Texas.

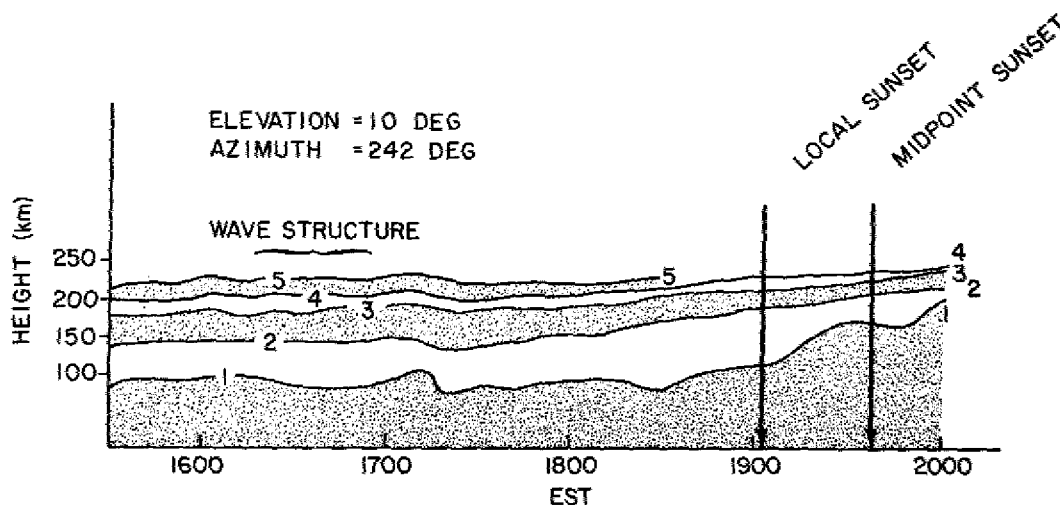


Fig. 17—Faraday-rotation isopleths obtained on May 19, 1970. An upward motion of an isopleth suggests a depletion in electron content, and a downward motion suggests a buildup in content. Isopleth 1 is the location of the point where Faraday rotation first becomes noticeable. It is referred to as the base of the ionosphere.

It has been shown (13) that the following order-of-magnitude relation holds:

$$-\frac{\delta h}{\tau} \sim \frac{\delta N}{N}, \quad (9)$$

where δh is the isopleth fluctuation, τ is the slab thickness to the height in question, N is the electron density, and δN is the electron-density fluctuation. Assuming that τ is ≈ 100 km and since δh was ≈ 10 km on May 19, Eq. (9) suggests that the relative density fluctuation is 10%. This figure is in line with the typical larger values of δN which have been obtained over Randle Cliff at small zenith angles (high elevation). In fact, during the period 1969-70, such measurements placed the average value of $\delta N/N$ at $\approx 4\%$ wherever wavelike disturbances were in evidence.

Also seen in Fig. 17 is a rather gradual ascent of the isopleths marked 2, 3, and 4 and a somewhat faster ascent of the isopleth marked 1. Since isopleth 1 symbolizes the lowest height in the ionosphere for which measureable ionization resides, one refers to it for convenience as the base of the ionosphere. Clearly the isopleth convergence is greater in the neighborhood of the ionospheric base than higher up in the F region. Thus one finds, not unexpectedly, that the lower portions of the ionosphere are highly favored as far as free-electron depletion is concerned.

Since an azimuth of 242 deg is generally westward, sunset effects would be expected to be temporally less advanced in the F -region portion of the ray path than in the E -region portion. Furthermore, it is well known that the F region is intrinsically more sluggish than the E region, for a fixed solar zenith angle. Both of these factors act together to produce a much greater effect in the E region than in the F region.

Figure 18 represents several Faraday-rotation isopleths for Oct. 28, 1970, as deduced by a CDC-3800 computer. The base of the ionosphere and the $\pi/2$ and the π rotation

isopleths are readily seen.* However, due to Faraday dispersion within the radar pulse, no other isopleths are visible. The thick region of data points residing between ≈ 250 and 300 km is simply the *F2* maximum. To see the behavior of the height of maximum ionization clearly, more extensive smoothing was performed, and the result is given in Fig. 19. The *F* layer would appear to exhibit an oscillation which, over a certain region, is roughly ± 10 km. However, this is not an isopleth fluctuation and consequently may not be as easily related to an electron-density fluctuation $\delta N/N$. (It is noteworthy that although a direct measurement of $\delta N/N$ could be made in principle, it was obviated in this experiment because of the deleterious effect of Faraday dispersion. To reduce the dispersive effect, it is planned for future tests to operate the radar at shorter pulse lengths at some sacrifice in signal-to-noise ratio.)

Other examples of *F*-layer height fluctuations are found in Figs. 20, 21, and 22 for observations on Feb. 24 and 26 and Mar. 3, 1971, respectively. It is remarked that some of the larger layer height fluctuations are probably related to atmospheric tidal motions and not to traveling ionospheric disturbances.

On Sept. 22, 1970, a combined HF-direction-finding (HF-DF) and Thomson scatter experiment was performed. HF-DF data were obtained at Hybla Valley, Virginia, from a source transmitter located at Galveston, Texas. Oblique-sounder group-path-delay data from both Lubbock and San Antonio, Texas, to Hybla Valley were also made available.† This data is discussed later in this report.

DISCUSSION OF THE THEORY OF LAYER HEIGHT FLUCTUATIONS

Ignoring the effects of small perturbations in electron production and loss through attachment, Hooke (14) finds that to first order the electron-density fluctuations due to the action of neutral gravity waves may be written as

$$-i\omega\delta N = (\mathbf{u} \cdot \hat{\mathbf{e}}_B) (\nabla N_0 \cdot \hat{\mathbf{e}}_B) + N_0 \nabla \cdot (\mathbf{u} \cdot \hat{\mathbf{e}}_B) \hat{\mathbf{e}}_B, \quad (10)$$

where N_0 is the ambient electron density, δN is a small perturbation, ω is the neutral-wave angular frequency, \mathbf{u} is the velocity of the gas, and $\hat{\mathbf{e}}_B$ is a unit vector directed along the magnetic field. This result represents basically only that portion of the ionospheric response which stems from dynamical processes. For use in this report Eq. (10) is simplified to

$$i\omega\delta N = -N_0 \nabla \cdot (\mathbf{u} \cdot \hat{\mathbf{e}}_B) \hat{\mathbf{e}}_B \quad (11)$$

by assuming that the ionization gradient is locally zero near the *F2* maximum in the limit of horizontal stratification. Equation (11) is not useful within the temporal neighborhood

*The computer routine searches for signal extrema. If the S/N is reasonably high, these extrema represent heights by which the amount of Faraday rotation is a multiple of $\pi/2$ radians. If S/N is low or if Faraday dispersion is large, a cluster of points appears near the true Faraday extremum. Near the *F2* maximum the Faraday extrema are close together, and dispersion renders a broad region of data points which define the location of the *F2* maximum rather well.

†Courtesy Messrs. M. Sheets and R. Gleason, Emitter Location Branch, Naval Research Laboratory, Washington, D.C.

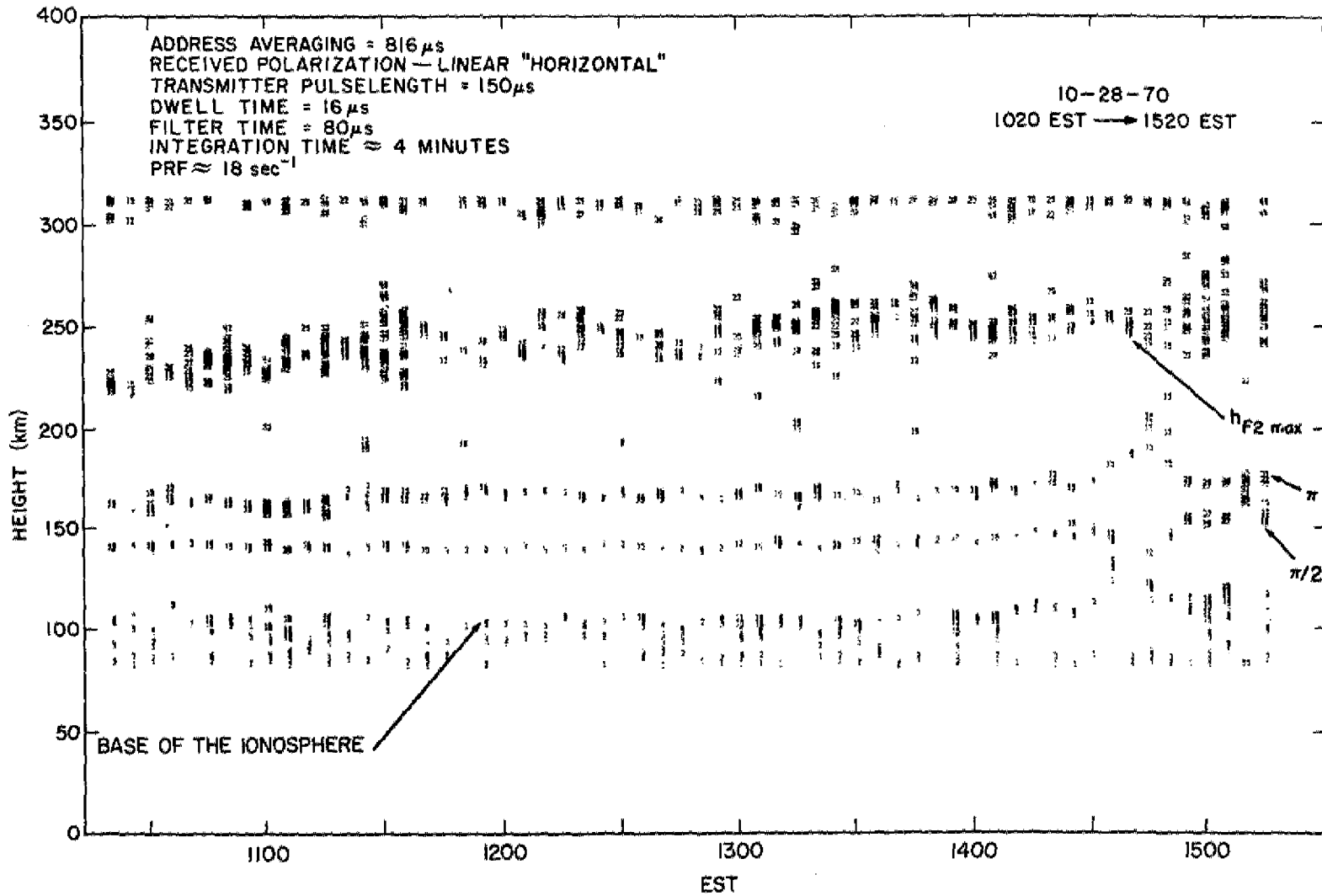


Fig. 18—Faraday-rotation isopleths obtained on Oct. 28, 1970. A range smoothing of $\approx 122 \text{ km}$ was applied. This corresponds to a height smoothing of $\approx 40 \text{ km}$ at the $F2$ maximum.

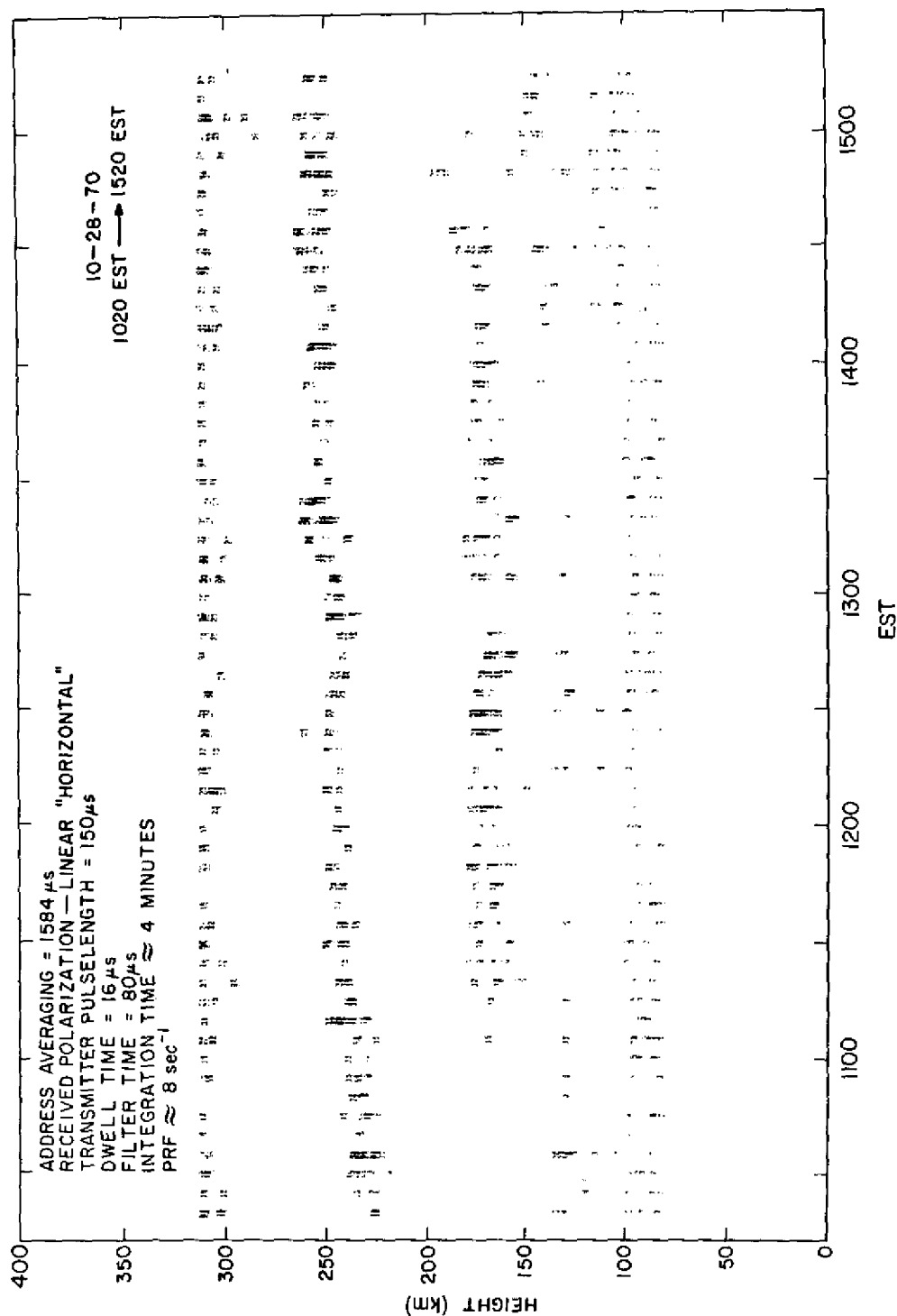


Fig. 19—Paraday-rotation isopleths obtained on Oct. 28, 1970. A range smoothing of \approx 238 km was applied. This corresponds to a height smoothing of \approx 77 km at the F2 maximum.

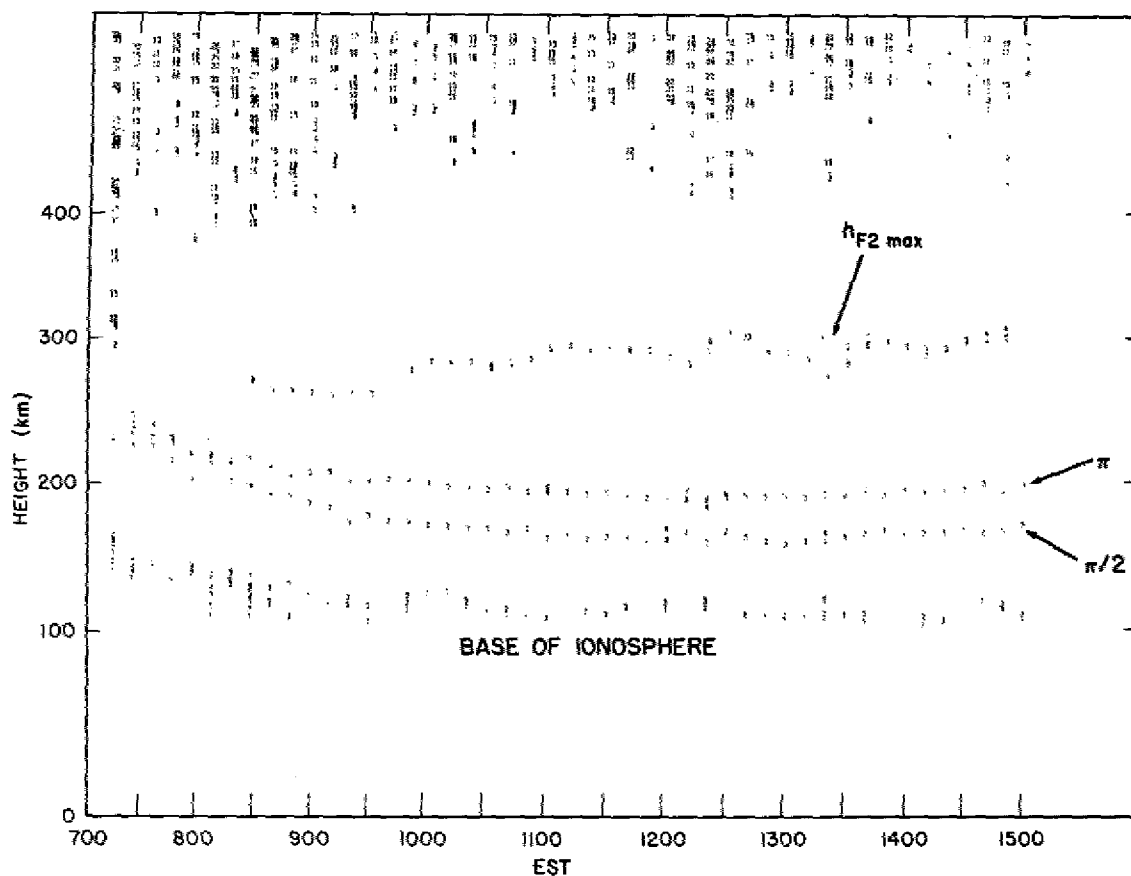


Fig. 20—*F*-layer height fluctuations observed on Feb. 24, 1971.

of sunrise or sunset when horizontal gradients are measurable and may also be inappropriate at high latitudes during disturbed periods. For simplicity the coordinate system is rotated so that the horizontal wave vector of the gravity wave is in the x direction. Furthermore, one allows for no wave dissipation along the horizontal, but one does permit wave amplification along the vertical. This simplification is required for conservation of energy and is of the form $\exp(k_{zi}z)$, where z is vertical distance. One notes that $k_{zi} \approx 1/2H$ according to free-wave theory as applied to an isothermal atmosphere (15). Thus the horizontal wave number k_x will be real, and the vertical wave number $k_z = k_{zr} + ik_{zi}$ will be complex. Under these conditions the fractional electron-density perturbation is expressed in terms of a vertical plasma displacement Z as,

$$\frac{\delta N}{N_0} = -Z \left(k_{zi} - \frac{ik_B}{\sin I} \right), \quad (12)$$

where $k_B = \mathbf{k} \cdot \hat{\mathbf{e}}_B$ is the component of the wave vector \mathbf{k} along the magnetic field \mathbf{B} whose direction is defined by the unit vector $\hat{\mathbf{e}}_B$ and I is the magnetic-inclination angle. Thus

$$\left| \frac{\delta N}{N_0} \right| = Z \left[k_{zi}^2 + \frac{k_B^2}{\sin^2 I} \right]^{1/2}, \quad (13)$$

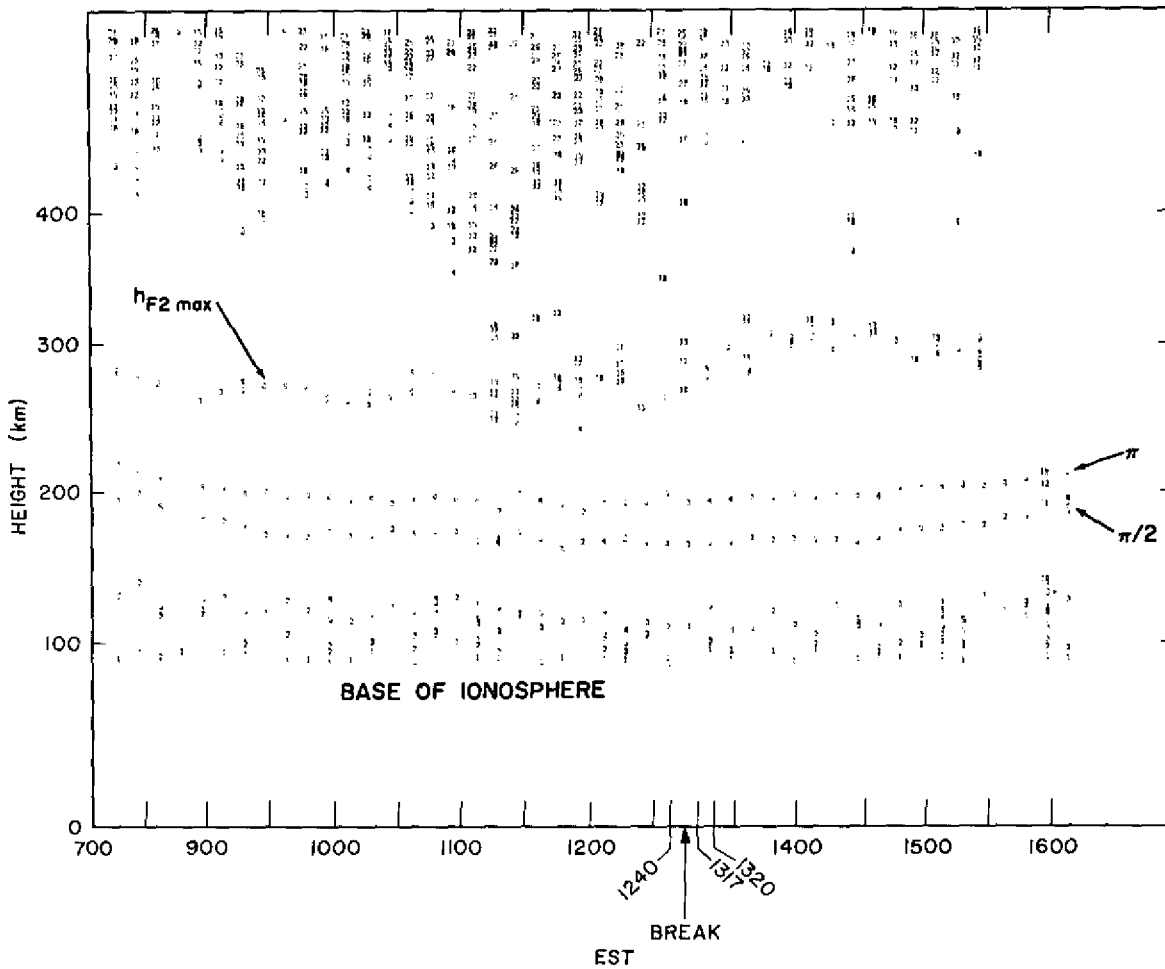


Fig. 21—F-layer height fluctuations observed on Feb. 26, 1971.

and

$$\left| \frac{\delta N}{N_0} \right| \geq \frac{Z}{2H} \tag{14}$$

according to internal-gravity-wave theory. Equation (14) affords a means to estimate the electron-density fluctuations within the framework of neutral-gravity-wave theory in an isothermal atmosphere. (In reality, of course, the atmosphere is not isothermal, and viscous dissipation must be taken into account.) Referring to Fig. 20 for which Z was observed to be $\approx \pm 10$ km, one finds that $\delta N/N$ would be greater than 20% on the basis of Eq. (14) and a neutral-scale-height assumption of 50 km. This fluctuation is rather large but not unreasonable, since such percentages have been observed by Thome (16) over Arcibo.

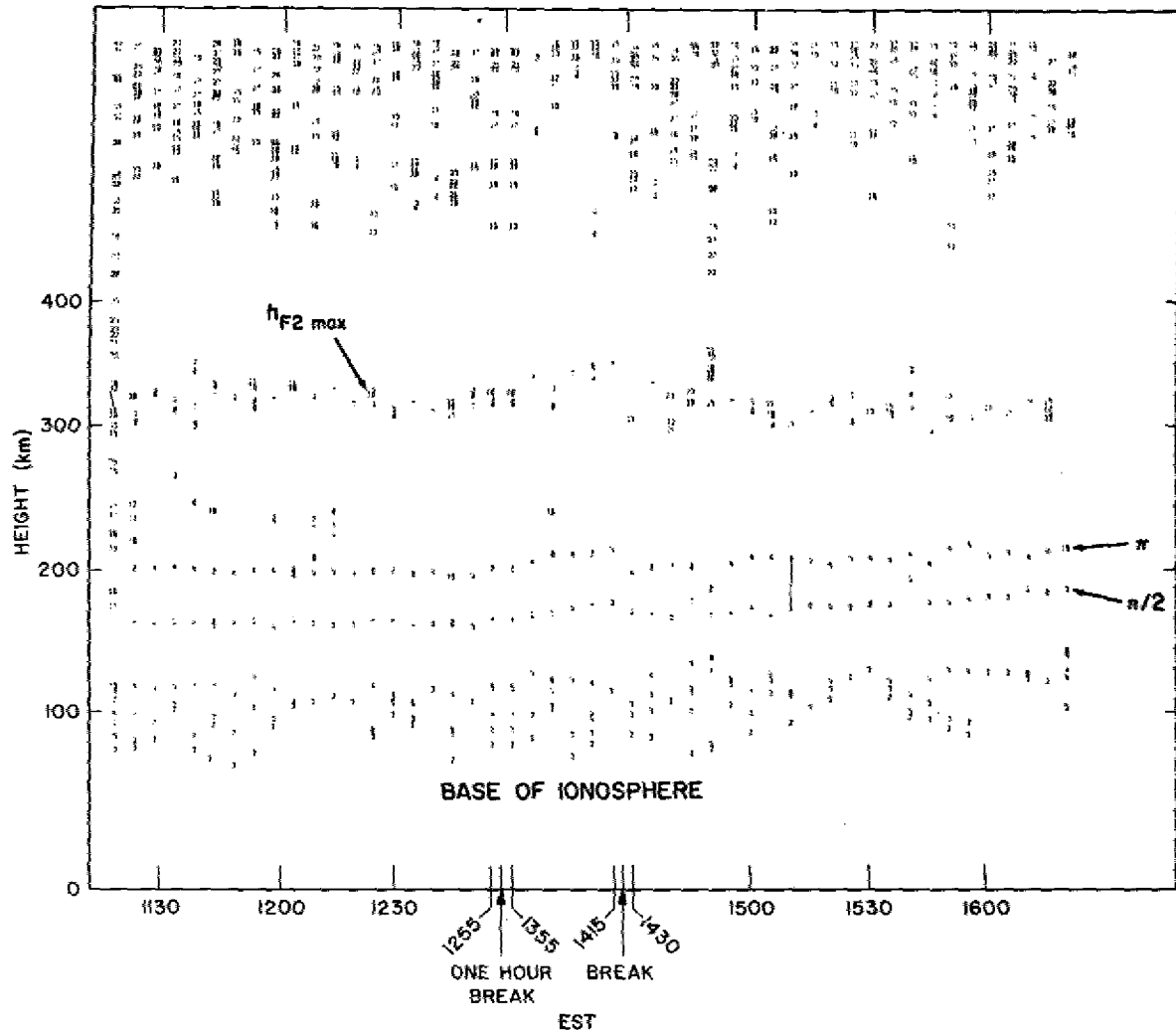


Fig. 22—*F*-layer height fluctuations observed on Mar. 3, 1971

COMPARISON OF OBSERVED BEARING-ANGLE FLUCTUATIONS AND THOSE PREDICTED USING THOMSON SCATTER

This section describes in some detail a set of data obtained on Sept. 22, 1970. Three types of information have been analyzed: VHF Thomson scatter, HF group-path delay, and HF angle-of-arrival data. The purpose of the analysis were (a) to exhibit correlations between the VHF and the HF data, and (b) to assess the ability of a Thomson scatter radar in providing data suitable for successful prediction of bearing-angle fluctuations.

Measurements

Between 0700 and 1930 EST on Sept. 22, 1970, Thomson scatter data were obtained using linear polarization.* During the initial phase of the measurement (0700-0900 EST), the antenna azimuth was 253 deg. During the central phase (0905-1800 EST), the azimuth was alternated between values of 246 deg (the approximate direction of San Antonio, Texas, as viewed from Randle Cliff) and 263 deg (the direction of Lubbock, Texas). During the terminal phase (1805-1930 EST), the azimuth was again set at 253 deg. Figures 23 and 24 display the raw data corresponding to the central phase of the experiment in isometric form. Figure 23 shows the 246-deg azimuth data (hereafter referred to as the VHF San Antonio data) for two smoothing conditions: 550 μ s and 1050 μ s. Figure 24 shows the 263-deg azimuth data (hereafter referred to as the VHF Lubbock data) for the same two smoothing conditions, which incidentally correspond to height smoothings of about 30 and 57 km respectively at the *F* region.

Three features are noteworthy on the isometric plots: (a) the obvious clutter peaks, (b) the Faraday-rotation extrema, and (c) the *F*2 maximum peak. Although the ratio of

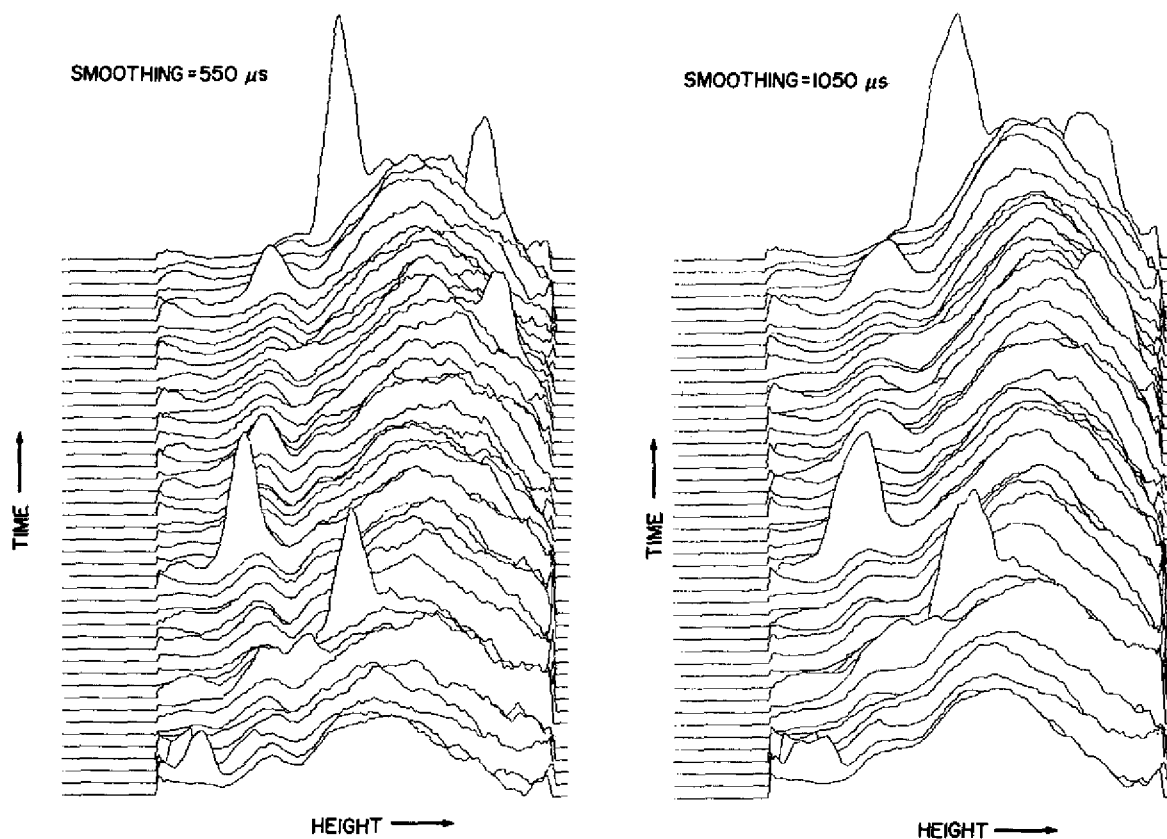


Fig. 23—Isometric plot of the VHF San Antonio data. The data were obtained 0905-1800 EST. Two smoothing conditions are employed.

*Table 3 gives the mean times and azimuths corresponding to the various Thomson scatter runs of Sept. 22, 1970.

Table 3
Mean Times Corresponding to Thomson Scatter Runs

Run	Azimuth (deg)	Time (EST)									
1	253	0702.5	40	246	1017.5	72	246	1317.5	111	263	1632.5
2	253	0707.5	41	263	1022.5	73	263	1322.5	112	246	1637.5
3	253	0712.5	42	246	1027.5	74	246	1327.5	113	263	1642.5
4	253	0717.5	43	263	1032.5	75	263	1332.5	114	246	1647.5
5	253	0722.5	44	246	1037.5	76	246	1337.5	115	263	1652.5
6	253	0727.5	45	263	1042.5	77	263	1342.5	116	246	1657.5
7	253	0732.5	46	246	1047.5	78	246	1347.5	117	263	1702.5
8	253	0737.5	*	*	*	79	263	1352.5	118	246	1707.5
9	253	0742.5	47	263	1058.5	80	246	1357.5	119	263	1712.5
10	253	0747.5	*	*	*	81	263	1402.5	120	246	1717.5
11	253	0752.5	48	246	1102.5	82	246	1407.5	121	263	1722.5
12	253	0757.5	49	263	1107.5	83	263	1412.5	122	246	1727.5
13	253	0802.5	50	246	1112.5	84	246	1417.5	123	263	1732.5
14	253	0807.5	*	*	*	85	263	1422.5	124	246	1737.5
15	253	0812.5	51	263	1124.5	86	246	1427.5	125	263	1742.5
16	253	0817.5	*	*	*	87	263	1432.5	126	246	1747.5
17	253	0822.5	52	246	1127.5	88	246	1437.5	127	263	1752.5
18	253	0827.5	53	263	1132.5	89	263	1442.5	128	246	1757.5
19	253	0832.5	54	246	1137.5	90	246	1447.5	129	263	1802.5
20	253	0837.5	55	263	1142.5	91	263	1452.5	130	253	1807.5
21	253	0842.5	*	*	*	92	246	1457.5	131	253	1812.5
22	253	0847.5	56	246	1154.5	93	263	1502.5	132	253	1817.5
23	253	0852.5	*	*	*	94	246	1507.8	133	253	1822.5
24	253	0857.5	57	263	1157.5	95	263	1512.5	134	253	1827.5
25	253	0902.5	58	246	1202.5	96	246	1517.5	135	253	1832.5
26	246	0907.5	59	263	1207.5	97	263	1522.5	136	253	1837.5
27	263	0912.5	60	246	1212.5	98	246	1527.5	137	253	1842.5
28	246	0917.5	*	*	*	99	263	1532.5	138	253	1847.5
29	263	0922.5	61	263	1222.5	100	246	1537.5	139	253	1852.5
30	246	0927.5	62	246	1227.5	101	263	1542.5	140	253	1857.5
31	263	0932.5	63	263	1232.5	102	246	1547.5	141	253	1902.5
32	246	0937.5	64	246	1237.5	103	263	1552.5	142	253	1907.5
33	263	0942.5	65	263	1242.5	104	246	1557.5	143	253	1912.5
34	246	0947.5	66	246	1247.5	105	263	1602.5	144	253	1917.5
35	263	0952.5	67	263	1252.5	106	246	1607.5	145	253	1922.5
36	246	0957.5	68	246	1257.5	107	263	1612.5	146	253	1927.5
37	263	1002.5	69	263	1302.5	108	246	1617.5	147	253	1932.5
38	246	1007.5	70	246	1307.5	109	263	1622.5			
39	263	1012.5	71	263	1312.5	110	246	1627.5			

San Antonio, Texas: Azimuth = 246 deg

Lubbock, Texas: Azimuth = 263 deg

Break in the data or an irregular sample interval: *

electron temperature to ion temperature and the effect of Faraday dispersion should be taken into account, it is also noted that the envelopes of the individual profiles are roughly indicative of the electron-density distribution of the ionosphere. In the F region the phenomenon of Faraday dispersion is essentially complete (the dispersion in polarization within a pulse is greater than π radians), and therefore the position of the $F2$ maximum is rather accurately placed. It has been shown in a recent paper (7) that F -layer height fluctuations could be related to the passage of traveling ionospheric disturbances, and that notion will be used in this report to extract estimates of bearing-angle fluctuations.

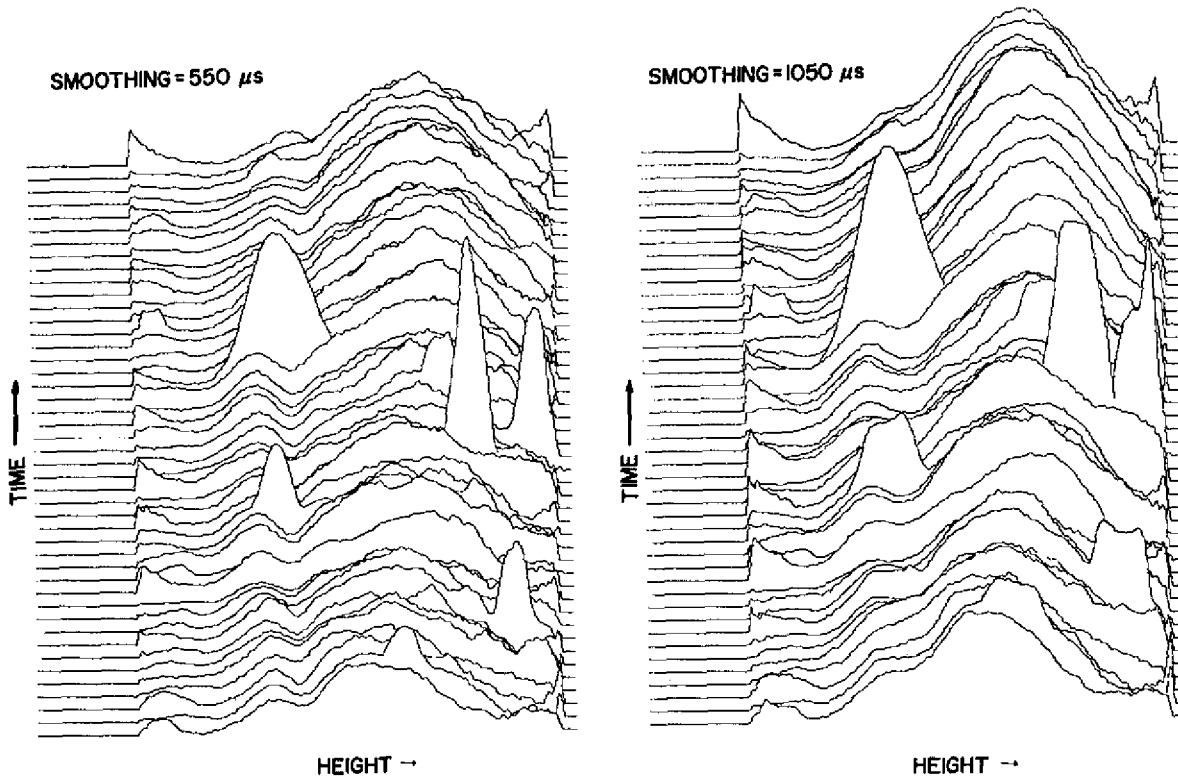


Fig. 24—Isometric plot of the VHF Lubbock data. The data were obtained 0905-1800 EST. Two smoothing conditions are employed.

Figures 25 and 26 are displays of the VHF San Antonio and VHF Lubbock data in a different form. The computer program which produced these displays was actually constructed to search for Faraday-rotation extrema on essentially noiseless data. It has been shown to work successfully during high-elevation runs and leads to the construction of Faraday-rotation isopleths (7). When this program is used for low-elevation data, however, only the first few extrema are legitimately Faraday-rotation extrema, and all others are due to other effects, noise, etc. Nevertheless, by applying sufficient smoothing it is possible to follow the motion of the largest extremum in the data (viz., the F^2 maximum) with greater ease than by examining the isometric plots of backscatter power. Of particular interest in Figs. 25 and 26 are the wakelike fluctuations which are seen. One can note that the fluctuations are less apparent until the amount of smoothing is increased. This is, of course, because of the presence of noise. Figure 27 is another version of the San Antonio data designed to allow the eye to follow the fluctuations more easily.

The region between 1015 and 1430 EST is particularly interesting, since during that period of time HF group-path-delay data have been made available. Figure 28 is a plot of the HF data which were obtained by measuring the time delay between signals sent from both San Antonio and Lubbock, Texas, and received at Hybla Valley, Virginia. Hybla Valley is approximately 66 km west of the Randle Cliff Radar facility. One clearly recognizes a fluctuation in group-path delay having a period of roughly 60 min. This periodicity is apparent in both the HF San Antonio and the HF Lubbock data, although there is a phase delay between the two. The fluctuation in group-path delay results from an oscillation in the height of ionospheric reflection which may be seen in the VHF data

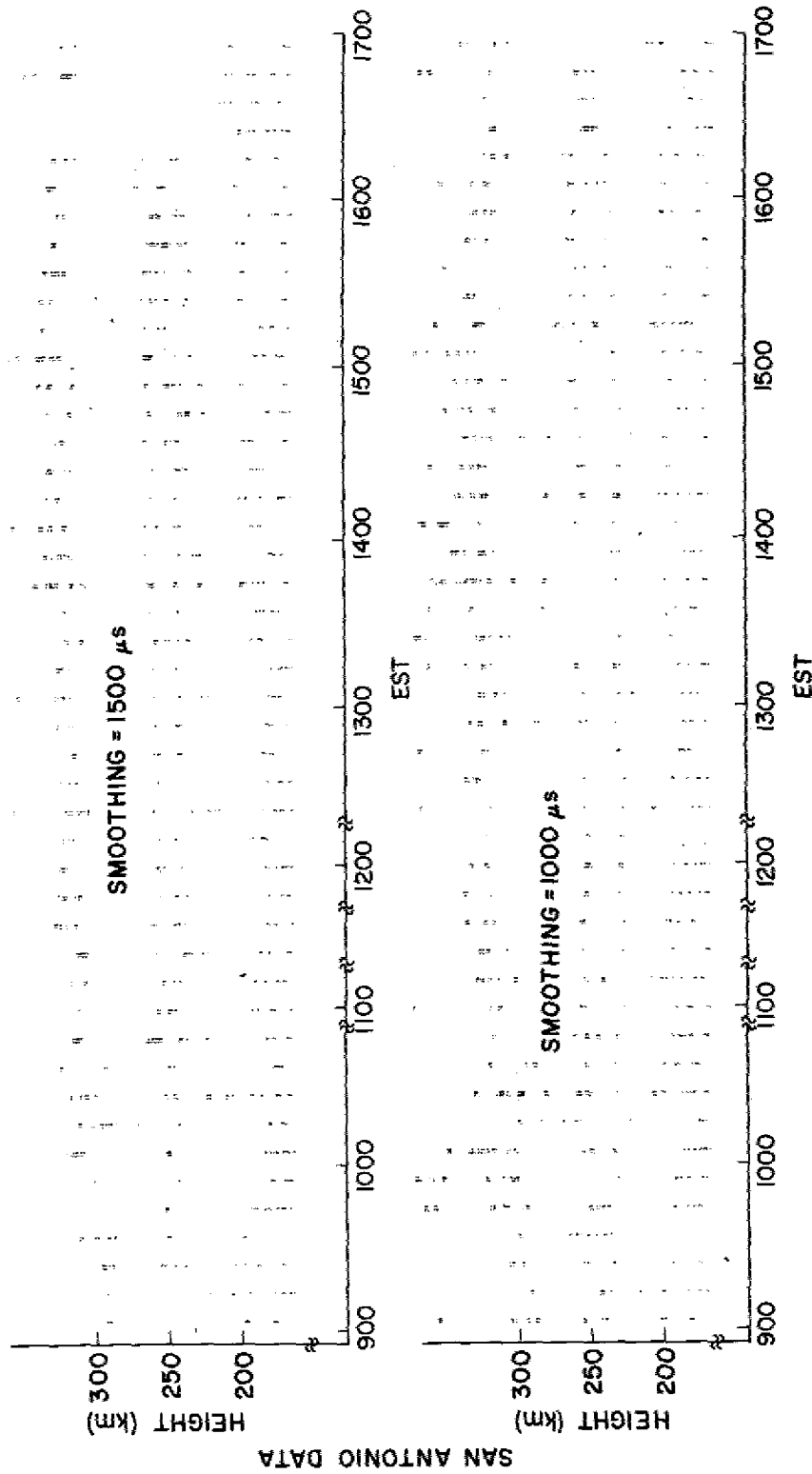


Fig. 25—Variation in the height of the F_2 maximum (upper region of points) for two conditions of smoothing. The other data points (below 300 km) are locations of Faraday extreme which have been disguised due to smoothing. VHF San Antonio data are depicted here.

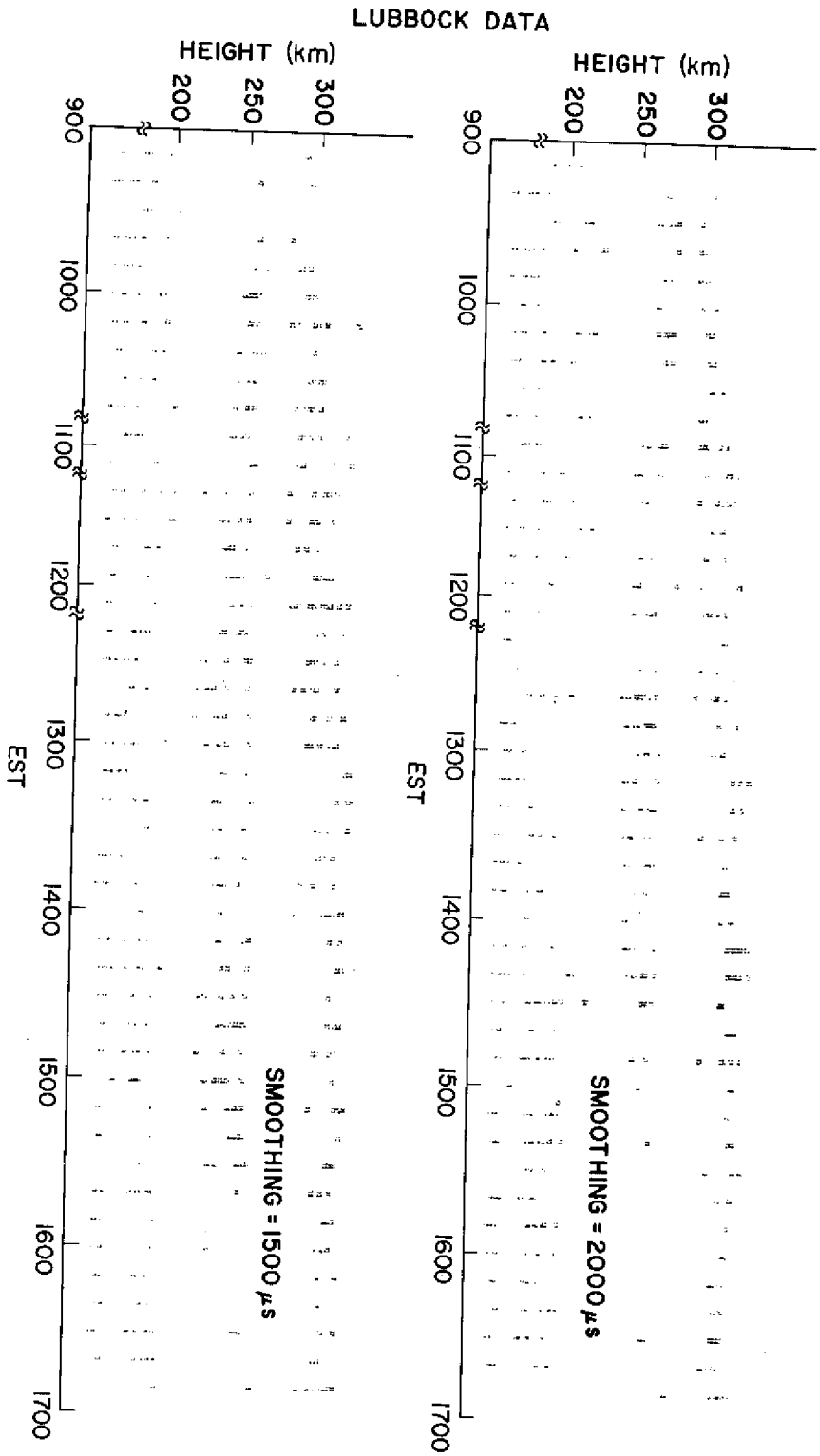


Fig. 26—Variation in the height of the F₂ maximum (upper region of points) for two conditions of smoothing. The other data points (below 300 km) are locations of Faraday extrema which have been disguised due to smoothing. VHF Lubbock data are depicted here.

THOMSON SCATTER RADAR DATA - 138.6 MHz
SAN ANTONIO DIRECTION MINUS 3° (ie., 246° @ NRL-CBD)
ELEVATION = 12°

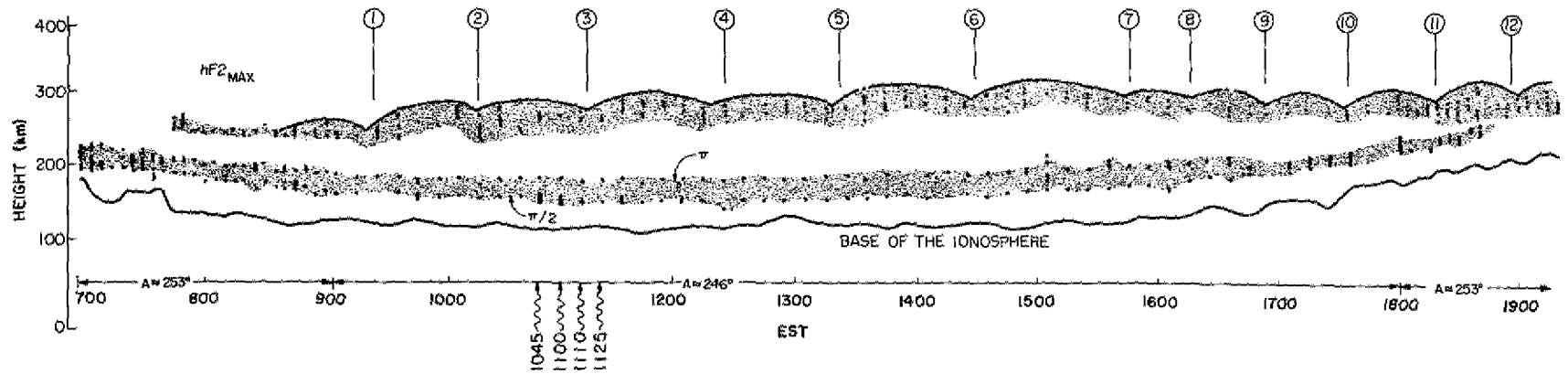


Fig. 27--F₂ maximum height fluctuations observed with Randle Cliff Radar pointing in the general direction of San Antonio, Texas. The region between the isopleths $\pi/2$ and π is also shaded.

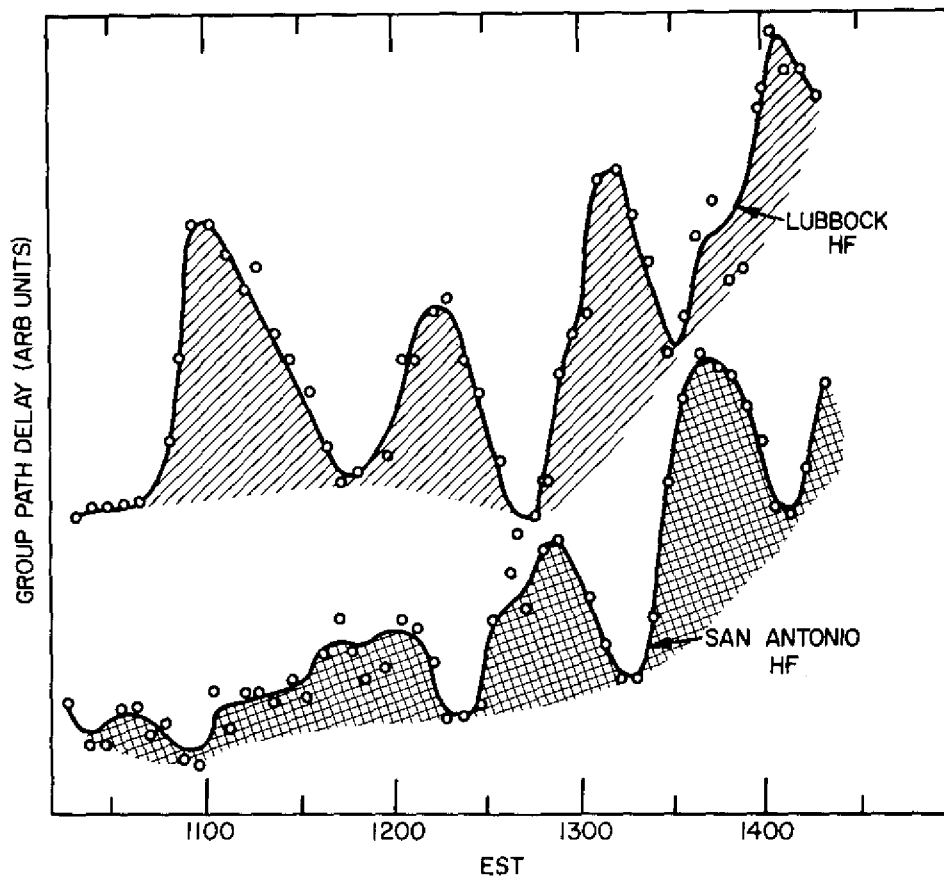


Fig. 28—Fluctuation in group-path delay at HF for signals sent from San Antonio and Lubbock, Texas, and received at Hybla Valley, Virginia

plotted in Fig. 29.* The F -layer oscillation is about ± 15 km and is felt to be caused by the passage of a traveling ionospheric disturbance. This TID is in turn generated as the ionospheric response to an internal gravity wave.

Figure 30 is a plan view showing the relative positions of the important sites corresponding to the HF and VHF experiments. The Lubbock paths would appear to be roughly the same in this view, whereas the San Antonio paths are different. The mid-points of the HF paths are depicted with stars, and the points at which the VHF radar path penetrates the F_2 maximum are shown with crosses. Also shown in the figure is the path connecting Hybla Valley, Virginia, and Galveston, Texas; over this circuit, HF bearing-angle data were obtained during the same period of time. For convenience one may refer to the midpoints of the HF paths directed toward San Antonio and Lubbock as the HF San Antonio and HF Lubbock points respectively. Similarly one may refer to the points where the VHF Thomson scatter ray penetrates the F_2 maximum in the directions of San Antonio (approximate) and Lubbock, Texas, as the VHF San Antonio and VHF Lubbock points respectively.

*The data points in Fig. 29 were obtained by computer averaging the clusters of points in the neighborhood of the F_2 maximum as depicted in Fig. 28.

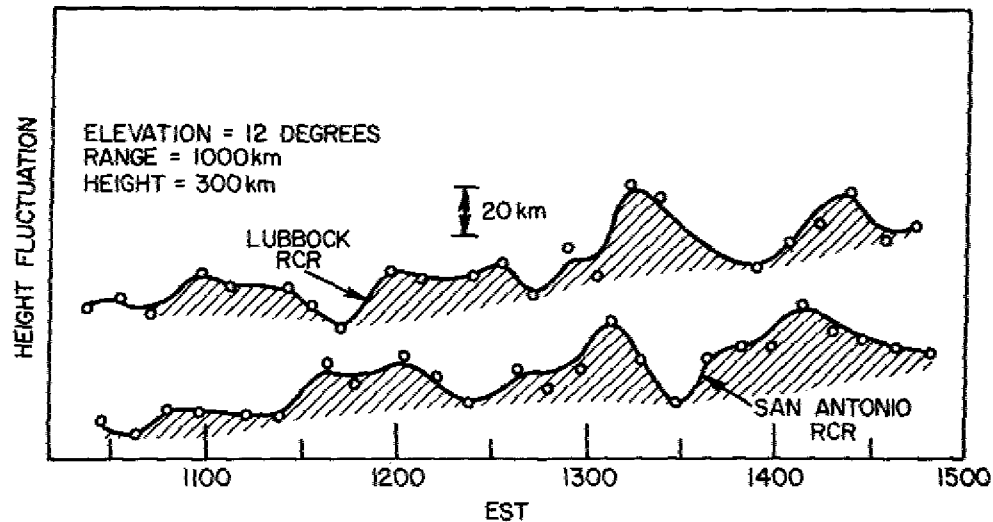


Fig. 29—F2 maximum height fluctuations obtained by averaging the clusters of points as depicted in Fig. 28. San Antonio and Lubbock data were used.

The positions of the stars and crosses in Fig. 30 are quite important, since it is on the basis of these differences that the phase delays between the various "waveforms" in Figs. 28 and 29 achieve real meaning. The lines joining the points shown in Fig. 30 approximate a parallelogram to first order with the distances $\alpha\beta$, $\beta\delta$, $\delta\gamma$, and $\gamma\alpha$ being ≈ 285 , ≈ 180 , ≈ 285 , and ≈ 200 km respectively. Figure 31 is a blown-up version of the parallelogram.

Figure 32 depicts the time delays between the four "waveforms" in Figs. 28 and 29. The arrows signify the comparisons which were made. The delays were extracted by superimposing the graphical data and sliding them with respect to one another until the best visual correlation was obtained between the waveforms. This procedure is felt to be as accurate as a computer cross-correlation approach, in view of the sampling accuracy of the data (10 min for the VHF case and 5 min for the HF case). Four situations are shown in Fig. 32: one for a wave assumed traveling northward, one for a wave traveling southward, one for a wave traveling westward, and one for a wave traveling westward.

In this analysis one assumes that the wavefront exhibits no curvature in the horizontal plane and that the basic shape of the wave train is roughly constant as it passes over the general region defined by the quasi-parallelogram $\alpha\beta\delta\gamma$. The east-west components of the vectors $\alpha\beta$, $\alpha\gamma$, $\beta\delta$, and $\gamma\delta$ are about equal. Hence one would expect that the phase lag between the observations at α and β , at α and γ , at β and δ , and at γ and δ would be comparable if the wave were moving in the east-west direction. Specifically one can require that the mathematical intersection of the temporal domains $t_{\alpha\beta}$, $t_{\alpha\delta}$, $t_{\beta\delta}$, and $t_{\gamma\delta}$ be nonvanishing, where the domains are defined as the stated time lag \pm the error. (The error of each time lag is taken to be plus or minus the sum of the two sampling resolutions corresponding to the two observation points on which the time lag is based. This is felt to be quite liberal.) For both westward and eastward waves,

$$(45, 75) \cap (12, 32) \cap (34, 64) \cap (2, 42) = 0 \quad (\text{westward})$$

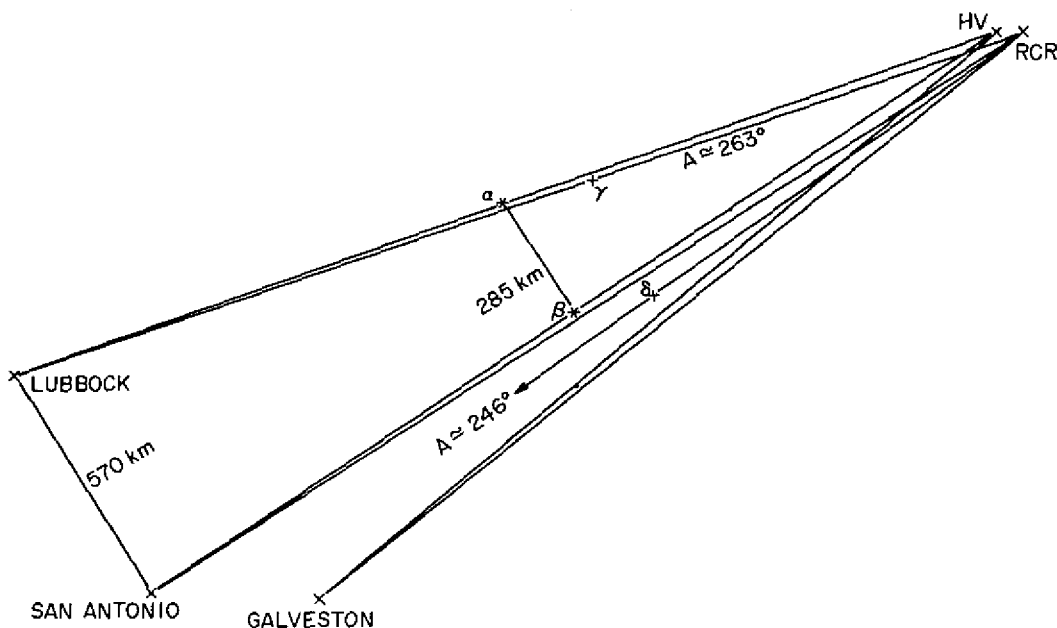


Fig. 30 — Relative positions of the important points corresponding to the HF and VHF experiments

and

$$(45, 75) \cap (24, 44) \cap (-4, 26) \cap (25, 68) = 0 \quad (\text{eastward})$$

respectively, where the symbol \cap represents intersection.

Although both intersections are zero, the westward case has vanishing intersections only by a narrow margin. Nevertheless since the east-west components of the vectors $\alpha\delta$ and $\beta\gamma$ have a ratio close to 10:1, one anticipates that $t_{\alpha\delta} \approx 10 t_{\beta\gamma}$. However, one finds that $t_{\alpha\delta} \approx 30 \pm 15$ and $t_{\beta\gamma} \approx 38 \pm 15$. Clearly the wave cannot be moving toward the west. Consequently on the basis of this simple analysis, one must assume that the wave exhibits basically a north-south motion.

From the geometry of the parallelogram in Fig. 30 (or Fig. 31), the north-south components of the vectors $\alpha\beta$ and $\gamma\delta$ are about equal, and the north-south components of $\alpha\gamma$ and $\beta\delta$ are about equal. Hence one can require that

$$(t_{\alpha\beta} \pm \theta_{\alpha\beta}) \cap (t_{\gamma\delta} \pm \theta_{\gamma\delta}) \neq 0 \quad (15a)$$

and

$$(t_{\alpha\gamma} \pm \theta_{\alpha\gamma}) \cap (t_{\beta\delta} \pm \theta_{\beta\delta}) \neq 0, \quad (15b)$$

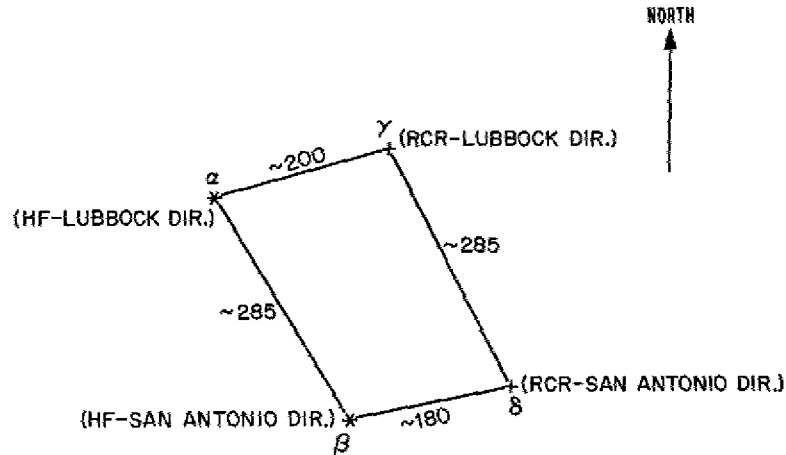


Fig. 31—Distances between corners of the parallelogram $\alpha\beta\gamma\delta$.

where θ_{ij} is the error associated with the pair of points i and j . Furthermore, one wants

$$t_{\gamma\delta} \approx t_{\alpha\beta} \approx 5t_{\beta\delta} \approx 5t_{\alpha\gamma}. \quad (16)$$

For a northward moving wave,

$$(t_{\alpha\beta} \pm \theta_{\alpha\beta}) \cap (t_{\gamma\delta} \pm \theta_{\gamma\delta}) = (10, 32) \cap (2, 44) \neq 0,$$

and

$$(t_{\alpha\gamma} \pm \theta_{\alpha\gamma}) \cap (t_{\beta\delta} \pm \theta_{\beta\delta}) = (-15, 15) \cap (-4, 26) \neq 0.$$

Also $t_{\gamma\delta} = 22 \pm 20$, $t_{\alpha\beta} = 22 \pm 10$, $t_{\beta\delta} = 11 \pm 15$, and $t_{\alpha\gamma} = 0 \pm 15$, so that Eq. (16) also holds to within the sampling-error limitation. Hence the wave could be moving toward the north.

For a southward moving wave, Eqs. (15a) and (15b) suggest that

$$(24, 44) \cap (25, 65) \neq 0$$

and

$$(-15, 15) \cap (-26, 4) \neq 0.$$

Furthermore, Eq. (16) also holds in this case, since $t_{\gamma\delta} = 45 \pm 20$, $t_{\alpha\beta} = 34 \pm 10$, $t_{\beta\delta} = -11 \pm 15$, and $t_{\alpha\gamma} = 0 \pm 15$. Hence the wave could be moving toward the south. Consequently one cannot determine whether the wave is moving north or south in a unique way; one only knows that it is not moving in the east-west direction. One suspects that the wave is moving toward the south, since $t_{\gamma\beta}$ is expected to be greater than $t_{\alpha\delta}$ for both northward and southward waves. But though this is true for a southward wave, it is not true for a northward wave if one ignores the error bars. Unfortunately the error bars are so broad that by suitable juggling it is possible to obtain the necessary ordering of the time lags. There are, however, other rather compelling reasons for preferring a southward wave. First, gravity waves have been shown to travel southward from

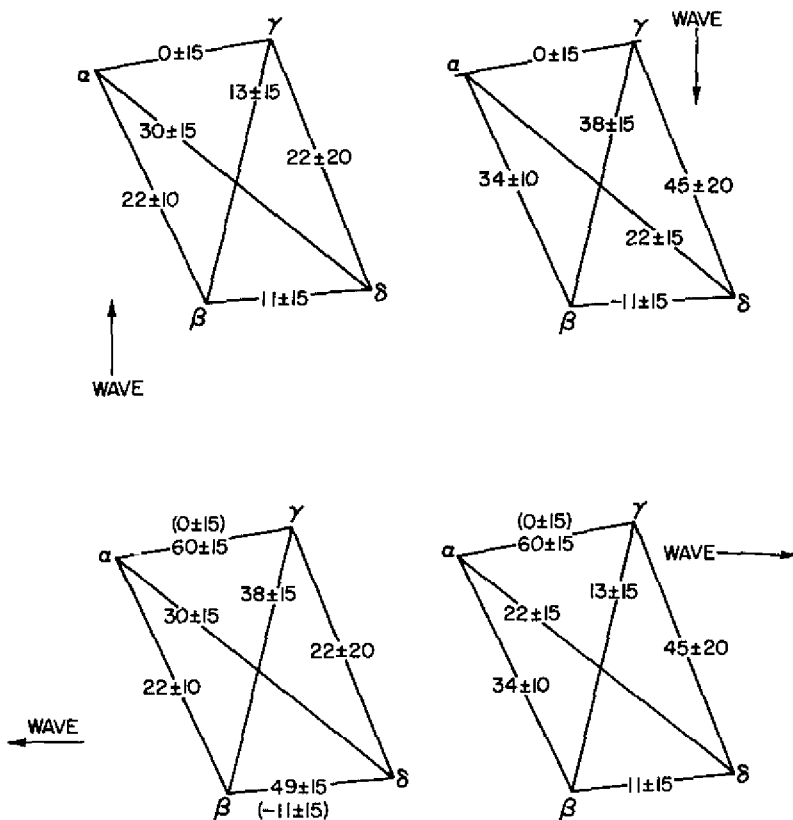


Fig. 32—Time lags between the various points and associated with northward, southward, eastward, and westward waves

the polar region, which acts as a source following magnetic activity. Second, ionospheric response to internal gravity waves is greater for southward waves than for northward waves.)

For a southward wave the distances between α and β and γ and δ are traversed in ≈ 40 min on the average; for a northward wave the distances are traversed in ≈ 22 min.* The north-south component of this distance is ≈ 240 km. Hence the north-south velocity of the disturbance is ≈ 6 km/min for a southward wave and ≈ 11 km/min for a northward wave. There is naturally a rather substantial uncertainty in this calculation; it is $\pm 27\%$ for the southward wave and $\pm 50\%$ for the northward wave.

*The average times are obtained as follows:

$$(t_{\alpha\beta} + t_{\gamma\delta})/2 = \bar{t}$$

The uncertainty in the average is taken to be:

$$\bar{\theta} \approx 1/2(\theta_{\alpha\beta}^2 + \theta_{\gamma\delta}^2)^{1/2}$$

Thus $\bar{\theta}/\bar{t}$ represents the fractional error.

The average wave period is ≈ 60 min; the horizontal wavelength is thus

$$\lambda_H \approx 360 \text{ km} \quad (\text{southward})$$

or

$$\lambda_H \approx 660 \text{ km} \quad (\text{northward}).$$

Since layer height fluctuations observed on September 22, 1970, were about ± 15 km and since H is close to 50 km, one may use Eq. (14) to estimate $|\delta N/N_0|$. One finds that $|\delta N/N_0| \geq 0.15$. Thus the relative change in the $F2$ maximum density must be greater than or equal to $\pm 15\%$. However since one has an estimate of λ_x it is possible to estimate $|\delta N/N_0|$ more accurately using Eq. (13). To arrive at an improved estimate, one must know something about the orientation of the wave vector \mathbf{k} . In the following one tries to estimate $\delta N/N_0$ on the basis of two approaches, one based on a surface wave and the other based on an internal gravity wave.

Figure 33 gives the geometry involved for both types of waves. It is possible to rewrite Eq. (12) as follows:

$$\delta N/N_0 = -Z[k_{zi} - ik(\sin \theta \cos \phi \cot I + \cos \theta)], \quad (17)$$

where ϕ is the azimuthal direction of the neutral wave (measured from the magnetic north), I is the magnetic inclination, θ is the angle between the horizontal and the lines of constant wave phase, k is the wave number, $k_{zi} = 1/2H$, and Z is the layer height fluctuation. For a surface gravity wave the lines of constant wave phase are vertical and,

$$\delta N/N_0 = -Z[k_{zi} - ik_H(\cos \phi \cot I)] \quad (18)$$

since $k = k_H$ and $\theta = 90^\circ$. On the other hand, for an internal gravity wave θ depends on the wave period, at least asymptotically. For an isothermal atmosphere with no dissipation, Tolstoy (17) has shown that

$$\theta = \tan^{-1} [\tau/\tau_B - 1]^{1/2}, \quad (19)$$

where τ_B is the Vaisala-Brunt period and τ is the gravity-wave period. Near the base of the thermosphere, τ_B is about 14 min, and $\tau \approx 60$ min in this study. Hence Eq. (19) yields a value for θ of $\approx 20^\circ$. Due to the effect of wave dissipation with increasing height, however, it is likely that Eq. (19) is an inappropriate description of the wave surfaces. In fact Hines (15) predicts a bending of the surfaces toward the vertical, and both Thome (18) and Goodman (13) have verified the fact experimentally. Nevertheless, Eq. (19) may be used as a lower limit for θ for the case of an internal gravity wave.

Rewriting Eq. (17) in terms of the horizontal wave number k_H , one has

$$\delta N/N_0 = -Z[k_{zi} - ik_H(\cot I \sec \phi + \cot \theta)], \quad (20)$$

where one has used the fact that $k_x = k \sin \theta \cos \phi$ and $k_H = k \sin \theta$. One may now estimate $\delta N/N_0$ from Eq. (18) (surface mode) and Eq. (20) (internal mode). Taking the wave to be traveling toward the south, one has $\phi = 180^\circ$, so that both $\sec \phi$ and $\cos \phi = -1$. The horizontal wavelength is ≈ 360 km or $k_H \approx 2\pi/360$. Although the interpretation of k_{zi} is rather complicated for surface modes (see Thome (16)), one shall take it to be the same as the internal gravity wave value; namely, $k_{zi} = 1/2H$ where H is the neutral

INTERNAL GRAVITY WAVES

SURFACE GRAVITY WAVES

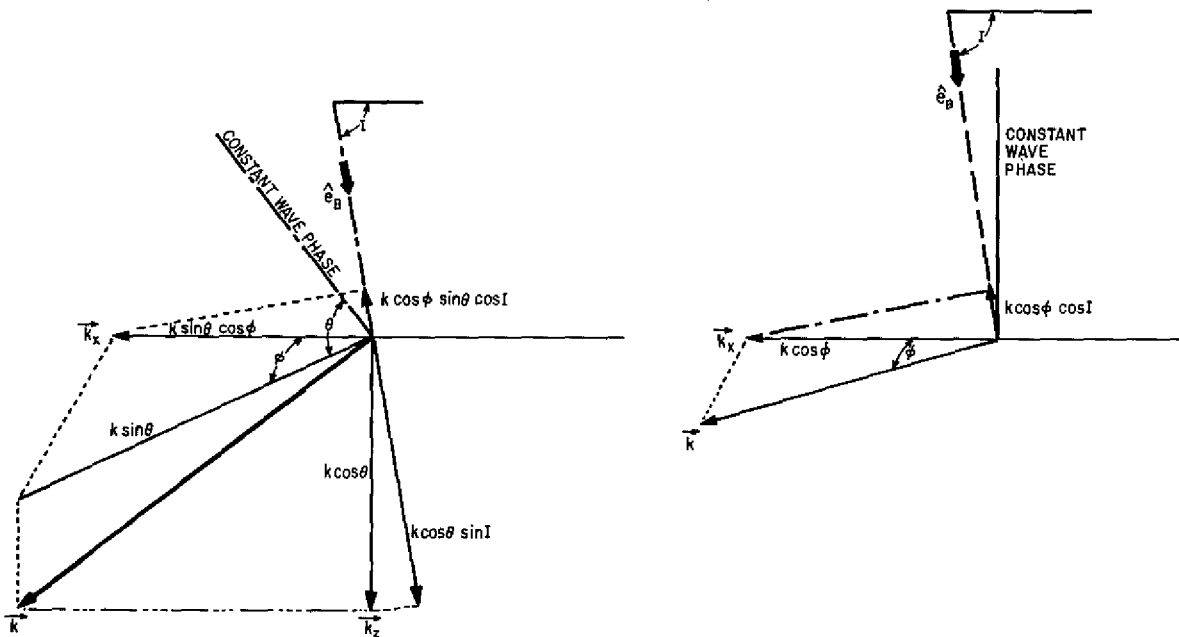


Fig. 33—Geometry of wave vectors and magnetic field for surface and internal gravity waves. I is the magnetic inclination, θ is the angle between the wave surfaces and the horizontal, \hat{e}_B is the direction of the magnetic field, and ϕ is the azimuthal direction of the wave (measured from north). The wave vector \mathbf{k} has a downward component for internal waves but is horizontal for surface waves.

scale height which is assumed to be 50 km near the $F2$ maximum. The magnetic inclination I is assumed to be 70° .

For a surface mode (Eq. (18)), one finds that $|\delta N/N_0| = 1.18 \times 10^{-2} \text{ km}^{-1} Z$ and for an internal mode (Eqs. (19) and (20)), one finds that $|\delta N/N_0| = 4.26 \times 10^{-2} \text{ km}^{-1} Z$. Since Z was observed to be $\approx \pm 15$ km, the surface wave would generate fluctuations in electron density of $\approx 18\%$, and the internal wave would generate fluctuations of $\approx 64\%$. Clearly the internal-gravity-wave estimate is ridiculously high. However this does not necessarily mean that the wave is of the surface variety. In fact, the phase speed of 6 km/min (or 100 m/s) is probably too low for a surface mode. Surface modes generally travel at an appreciable fraction of the local acoustic velocity (nearly 700 m/s in the F region). If viscous dissipation were taken into account, it is possible that θ could become quite large especially in the upper F region. Discarding Eq. (19) and taking $\theta = 70^\circ$, for example, one finds that the imaginary term in Eq. (20) vanishes, so that $|\delta N/N_0| = k_{zi} Z = 1 \times 10^{-2} \text{ km}^{-1} Z$ and the fluctuations in electron density would be $\approx 15\%$.

Without wavefront tilt measurements, one finds that it is not possible to evaluate the imaginary term $k_B \sin I$. However one suspects that the wave which produced the traveling ionospheric disturbance and the layer height fluctuations was an internal gravity wave which was severely modified by viscous dissipation. Other measurements of traveling disturbances over Randle Cliff suggest that wave periods of 60 min are associated with perturbations in electron density, which are roughly out of phase with the layer height fluctuations. This condition may be fulfilled if the surfaces of constant wave phase are lined up with the magnetic field. Surface waves are to within 20° of satisfying this requirement at Randle Cliff, and it is possible that dissipated internal gravity waves may also come close provided that they travel from north to south.

In the following discussion, one shall tacitly assume that $|\delta N/N_0| = k_{zi} Z$, where $k_{zi} = 10^{-2} \text{ km}^{-1}$. That is, one shall ignore the imaginary term $ik_B/\sin I$ as though $\theta = 70^\circ$. One shall subsequently find that this assumption appears quite reasonable. Thus one shall assume that the layer height fluctuations of 15 km are associated with electron-density fluctuations. Although this perturbation may be the result of either a northward or southward moving wave, there are compelling reasons for choosing the latter. The perturbation may be associated with unsettled magnetic activity observed at Fredericksburg on the preceding night. Table 4 shows the K_{FR} indices for Sept. 21 and 22, 1970. The distance between the north magnetic pole and the set of observation points is about 4300 km. For a wave velocity of 360 km/hr (6 km/min), 12 hr would be required to traverse this distance. One notes that a generally unsettled period of magnetic activity occurred ≥ 12 hr prior to the median observation time. The suggestion is that this magnetic activity may have triggered an oscillation responsible for the reported observations. It is emphasized that this argument is rather tenuous in the rigorous sense; it does, however, give added weight to the notion of a strictly southward wave. Table 5 is a list of the pertinent parameters of the wave which have thus far been deduced.

Table 4
 K_{FR} Indices for Sept. 21 and 22, 1970

Median Time (UT)	Time (local)	K_{FR}
1.5 Sept. 21	20.5 Sept. 21	3
4.5 Sept. 21	23.5 Sept. 21	3
7.5 Sept. 21	2.5 Sept. 21	4
10.5 Sept. 21	5.5 Sept. 21	2
13.5 Sept. 21	8.5 Sept. 21	4
16.5 Sept. 21	11.5 Sept. 21	3
19.5 Sept. 21	14.5 Sept. 21	2
22.5 Sept. 21	17.5 Sept. 21	3
1.5 Sept. 22	20.5 Sept. 21	3
4.5 Sept. 22	23.5 Sept. 21	3
7.5 Sept. 22	2.5 Sept. 22	1
10.5 Sept. 22	5.5 Sept. 22	2
13.5 Sept. 22	8.5 Sept. 22	1
16.5 Sept. 22	11.5 Sept. 22	2
19.5 Sept. 22	14.5 Sept. 22	2
22.5 Sept. 22	17.5 Sept. 22	2

} Unsettled period
 ↑
 12 hr
 ↓
 Median time

Transformation of Wave Parameters into Predicted Bearing Angle

It has been shown that the following relation is useful in predicting the electron-density fluctuation $\delta N/N_0$ arising from an internal gravity wave:

$$\delta N/N_0 = -k_{zi} Z$$

where $k_{zi} \approx 10^{-2} \text{ km}^{-1}$ and Z is the layer height fluctuation in km.

Thus the F -layer height fluctuations are inversely proportional to the electron-density fluctuations. Furthermore, since the F -layer height fluctuations are associated with a traveling wave, $\delta N/N_0$ must be oscillatory in both space and time. The result is that time-varying electron-density gradients may be constructed in the direction transverse to the

Table 5
Wave Parameters

Parameter	Symbol	Units	Value
Fractional Perturbation in Electron Density	$\delta N/N_0$	—	± 0.15
F2 Maximum Height Fluctuation	Z	km	± 15
Direction	—	—	Southward
Velocity	V_x	km/min	6
Period	P	min	60
Horizontal Wavelength	λ_x	km	360

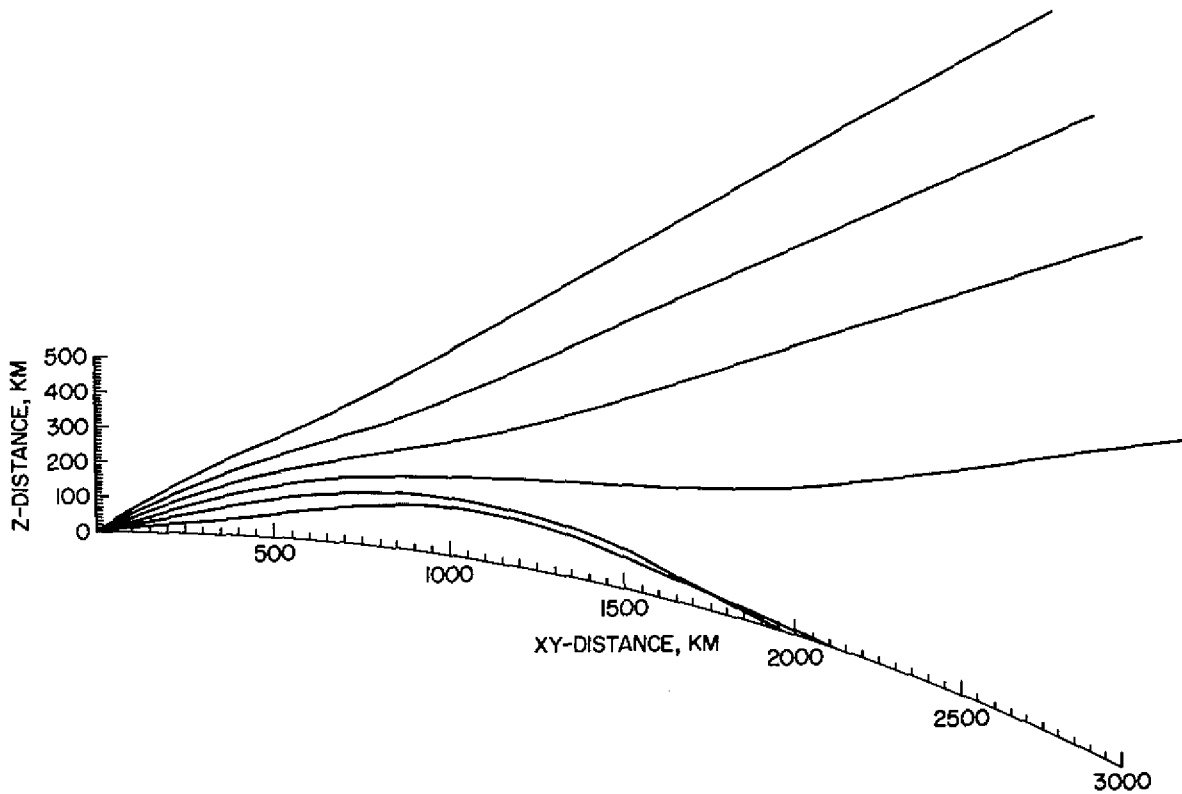


Fig. 34—Ray trace showing the trajectories of six rays launched at elevation angles of 5, 10, 15, 20, 25, and 30 deg. A radio frequency of 19.0 MHz is used, and the electron-density profile is based on a standard ionospheric model below the *E* region and in the upper *F* region and on an observed distribution in the critical intervening region.